

Sensitivity enhancement in solution NMR: Emerging ideas and new frontiers

Jung Ho Lee, Yusuke Okuno, Silvia Cavagnero*

Department of Chemistry and Biophysics Program, University of Wisconsin-Madison, 1101 University Avenue, Madison, WI 53706-1322, USA

ARTICLE INFO

Article history:

Received 25 October 2013

Revised 14 January 2014

Keywords:

NMR sensitivity
Hyperpolarization
Dissolution DNP
Overhauser DNP
Photo-CIDNP
PHIP
SEOP
Fast NMR

ABSTRACT

Modern NMR spectroscopy has reached an unprecedented level of sophistication in the determination of biomolecular structure and dynamics at atomic resolution in liquids. However, the sensitivity of this technique is still too low to solve a variety of cutting-edge biological problems in solution, especially those that involve viscous samples, very large biomolecules or aggregation-prone systems that need to be kept at low concentration. Despite the challenges, a variety of efforts have been carried out over the years to increase sensitivity of NMR spectroscopy in liquids. This review discusses basic concepts, recent developments and future opportunities in this exciting area of research.

© 2014 Elsevier Inc. All rights reserved.

1. Basic concepts and well-established advances

1.1. Fundamental concepts

While early nuclear magnetic resonance observations were performed on bulk materials and simple molecules such as paraffin and water [1], the technique has now become much more sophisticated and NMR data are routinely collected in solution on dilute biological macromolecules at concentrations typically ranging from 100 μ M to 10 mM. The atomic resolution of NMR spectroscopy and its high information content, which includes both structure and dynamics in solution [2], render it an exceptional tool in biology. Yet the poor sensitivity of NMR is still a challenge.

For spin-1/2 nuclei, the magnetization, which is proportional to the NMR resonance intensity (i.e., the signal), can be generally defined as

$$M = \frac{\gamma \hbar N}{2} P, \quad (1)$$

where γ denotes the nuclear gyromagnetic ratio, \hbar is the Planck's constant divided by 2π , N is the total number of spins, and P is the nuclear polarization, defined as

$$P = \frac{N_\alpha - N_\beta}{N_\alpha + N_\beta} = \frac{N_\alpha - N_\beta}{N}, \quad (2)$$

where N_α and N_β are the number of α and β spins, respectively. It is useful to keep in mind that P is often expressed as a percent polarization $P\%$, with $P\% = P \times 100$.

At thermal equilibrium, the Boltzmann distribution applies, and the above relations can be expressed as

$$P = \frac{N_\alpha - N_\beta}{N_\alpha + N_\beta} = \frac{\exp\left(\frac{\gamma \hbar B_0}{2k_B T}\right) - \exp\left(-\frac{\gamma \hbar B_0}{2k_B T}\right)}{\exp\left(\frac{\gamma \hbar B_0}{2k_B T}\right) + \exp\left(-\frac{\gamma \hbar B_0}{2k_B T}\right)} = \tanh\left(\frac{\gamma \hbar B_0}{2k_B T}\right), \quad (3)$$

where T is the absolute temperature, B_0 is the applied magnetic field and k_B is the Boltzmann constant [3]. At physiologically relevant temperatures, $P\%$ is extremely small even at very high applied fields. For instance, the ^1H percent polarization in a 1000 MHz NMR spectrometer is only 0.008% at room temperature.

Despite the small intrinsic polarization, spectroscopic sensitivity can be high if the noise level is small. This concept follows from the definition of sensitivity [4] expressed as signal-to-noise per unit time

$$\left(\frac{S}{N}\right)_t = \frac{S}{2\sigma_N \sqrt{t}} \cong \frac{2.5 \times S}{\langle N_{\text{ptp}} \rangle \sqrt{t}}. \quad (4)$$

In the above relation, S is the signal peak amplitude, t is the total NMR experimental time, σ_N is the r.m.s. noise amplitude, and $\langle N_{\text{ptp}} \rangle$ is the peak-to-peak noise amplitude within 100 zero crossings,

* Corresponding author. Address: Department of Chemistry, University of Wisconsin-Madison, 1101 University Avenue, Madison, WI 53706, USA. Fax: +1 608 262 9918.

E-mail address: cavagnero@chem.wisc.edu (S. Cavagnero).

where $\langle N_{\text{ptp}} \rangle \cong 5.0 \sigma_N$ [4]. Here, the term amplitude is regarded as equivalent to height. Note that both S and σ_N are known to be intrinsically time-dependent and to increase linearly with t and \sqrt{t} , respectively [4]. Therefore, dividing the signal-to-noise ratio by \sqrt{t} in Eq. (4) renders the NMR sensitivity $(S/N)_t$ independent of the total experimental time.

A more explicit description of the magnetic field (B_0) and gyromagnetic ratio (γ) dependence of the signal-to-noise S/N can be obtained upon considering: 1) the relation $M \propto \gamma^2 B_0$, which is evident from Eqs. (1) and (3) when $\frac{\gamma \hbar B_0}{2k_B T} \ll 1$, 2) the linear dependence of the voltage measured across the NMR receiver coil on γB_0 , i.e., the magnetization oscillation frequency, and 3) the noise dependence on $(\gamma B_0)^{1/2}$. The combination of the above effects yields [5–7]

$$\left(\frac{S}{N}\right) \sim \frac{(\gamma^2 B_0)(\gamma B_0)}{(\gamma B_0)^{1/2}} \sim B_0^{3/2} \gamma^{5/2}. \quad (5)$$

Note that, depending on different assumptions on noise level and instrumental factors, slightly different B_0 and γ power dependencies of S/N have in some cases been reported [8,9].

Remarkably, a number of key advances in NMR over the last few decades led to remarkable improvements in sensitivity. As a result, the current sensitivity of NMR spectroscopy is not so different from that of other techniques characterized by much more favorable Boltzmann factors (e.g., electron paramagnetic resonance, infrared spectroscopy). However, NMR sensitivity is currently largely inferior to that of other spectroscopic techniques, e.g., fluorescence, whose detection limit has recently been stretched down to the single-molecule level. This review documents ongoing efforts to render solution NMR a more sensitive technique, with emphasis on biomolecular applications.

1.2. Some well-established advances

Given that the NMR signal-to-noise increases nonlinearly with magnetic field B_0 (i.e., proportional to $\sim B_0^{3/2}$, see Eq. (5)), high applied magnetic fields have been traditionally recognized as the most straightforward means to enhance NMR sensitivity. The introduction of superconducting magnets paved the way to enhanced spin polarization at very high fields, nowadays reaching up to 23.5 T (corresponding to 1000 MHz). In addition, Fourier-transform pulsed NMR, delivering short radiofrequency pulses covering a wide range of excitation frequencies at once, eliminated the need for frequency scanning and enabled the fast accumulation of multiple transients in a short time, leading to a dramatic ≥ 100 -fold increase in sensitivity [4]. Receiver coils composed of materials with very small magnetic susceptibility enabled minimal magnetic field distortions, improving lineshapes and signal-to-noise. The active sample volume has also increased due to improvements in shimming technology, leading to a larger number of detectable NMR-active nuclei [10]. The use of analog filters in combination with time-domain oversampling followed by digital filtering led to the elimination of aliased noise, contributing to improved sensitivity [3,10]. Recently, the introduction of cryogenic probes led to a significant reduction in noise level via cooling of receiver coils and preamplifiers down to approximately 20 K and 80 K, respectively [11].

Heteronuclear NOE (Nuclear Overhauser Effect) [12] can be employed when sensitive and insensitive nuclei are in close spatial proximity. For instance, ^1H saturation, producing steady-state NOE, leads to higher ^{13}C sensitivity. In addition, INEPT (Insensitive Nuclei Enhanced by Polarization Transfer) [13] pulse scheme can be used to transfer magnetization from sensitive to insensitive nuclei in the presence of scalar coupling between the two. In many heteronuclear pulse sequences, INEPT is followed by reverse INEPT

(transfer of magnetization back to the sensitive nuclei for detection). Here, the Preservation of Equivalent Pathways (PEP) method [14] can be used to gain sensitivity improvements by factors up to $\sqrt{2}$ relative to the typical reverse INEPT.

Various isotopic labeling strategies were recently developed to maximize NMR sensitivity and resolution in large biomolecules or complex mixtures [15,16]. ^{13}C - and ^{15}N -enriched biomolecules are no longer limited by natural abundance, and ^2H -enrichment leads to reduced dipolar cross-relaxation and spin diffusion [17]. NMR pulse sequences tailored to these isotope labeling schemes have rendered them maximally useful [2,18]. In addition, NMR tubes matching the susceptibility of the glass to that of water (e.g., Shigemi tubes) and specialized microcoil/small-volume sample-tube setups help maximizing NMR sensitivity in experiments limited by small amounts of material [19,20].

2. Methods taking advantage of relaxation rates and chemical shift evolution

2.1. Sensitivity enhancement via fast pulsing techniques

Reduction of data collection time to achieve a given S/N is a powerful strategy to enhance NMR sensitivity. Pulse sequences belonging to the SOFAST HMQC class [21,22] enable fast pulsing by combining multiple strategies to shorten experiment time without significant losses in S/N . First, selective excitation of amide protons leads to fast $^1\text{H}^N$ T_1 relaxation since auto-relaxation is not efficiently compensated by cross-relaxation for slow-tumbling biomolecules in the $\omega_o \tau_c \gg 1$ regime [23,24], where ω_o is the Larmor frequency and τ_c is the rotational correlation time. Second, Ernst-angle excitation is employed to maximize signal-to-noise per unit time [4]. Both of the above strategies enable dramatic reductions in recycle delay duration. Lastly, the HMQC pulse sequence [25] is employed to minimize the number of selective pulses.

2.2. Sensitivity enhancement by attenuation of T_2 relaxation

As seen in Eq. (4), the NMR sensitivity $(S/N)_t$ is directly proportional to signal peak height. Thus, efforts to sharpen NMR resonances by decreasing linewidths (and consequently increasing peak heights) can be regarded as NMR sensitivity enhancement tools. This topic becomes particularly pressing in the case of large biomolecules, characterized by extensive resonance linebroadening.

Linebroadening resulting from large molecular size can be mitigated by Transverse Relaxation Optimized Spectroscopy (TROSY). This method increases the effective spin-spin relaxation time T_2 by selecting the longest-lived coherences resulting from the mutual cancellation of chemical shift anisotropy (CSA) and dipolar relaxation effects [26] or between ^1H – ^1H and ^1H – ^{13}C dipolar relaxation mechanisms [27]. For instance, when sequential backbone assignments were carried out on the octameric 110 kDa protein 7,8-dihydroneopterin aldolase with both conventional HNCA and [^{15}N , ^1H]-TROSY-HNCA, a 20- to 50-fold higher sensitivity was achieved with the TROSY-type experiment [28].

In case linebroadening is caused by conformational exchange, “chemical shift scaling” [29] can be used to shift the exchange regime from intermediate to fast on the NMR chemical shift timescale, leading to sharper linewidths [30,31]. This concept can be implemented by applying the CPMG [32] or WAHUHA [33] based four-pulse trains during the chemical shift evolution time.

The methods described so far start from a Boltzmann distribution of nuclear spin states. In contrast, methods able to shift the thermal nuclear spin populations, illustrated in Fig. 1 and compared in Table 1, provide an alternative avenue to enhance NMR

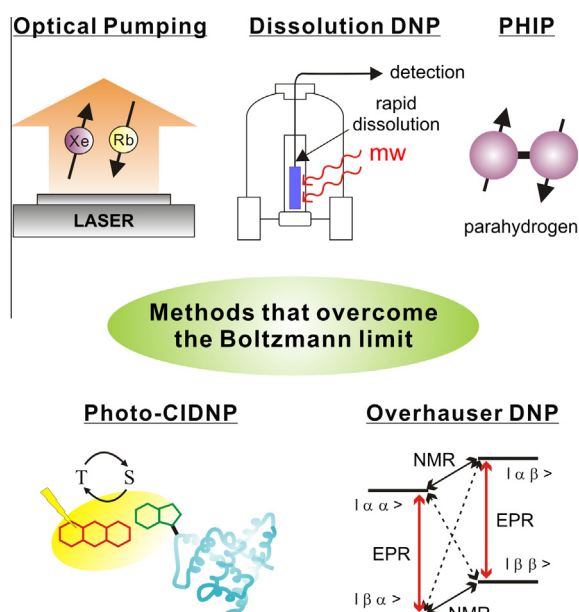


Fig. 1. Overview of methods that perturb the longitudinal magnetization of nuclear spins in solution.

sensitivity. It is important to note that strategies to increase NMR sensitivity usually add up in a cumulative fashion, leading to the current state-of-the-art. This idea suggests that further advances, including those outlined in the following sections, will not replace but rather improve the current status quo.

3. Dissolution dynamic nuclear polarization

3.1. Basic concepts

A recently developed approach known as dissolution DNP [37] creatively exploits dynamic nuclear polarization (DNP), a well-known phenomenon leading to hyperpolarized NMR-active nuclei in the solid state. Given that dissolution DNP involves NMR analysis of liquids, this technique is suitable to study water-soluble biologically relevant samples. This method has become quite popular over the last few years, and dissolution DNP setups are now commercially available (e.g. HyperSense from Oxford Instruments).

In short, a solid, frozen-solution sample at very low temperature (typically 1.1–1.5 K) is polarized in the presence of a radical, e.g. tris {8-carboxyl-2,2,6,6-tetra[2-(1-hydroxyethyl)]-benzo(1,2-d:4,5-d')bis(1,3)dithiole-4-yl} methyl sodium salt (Trityl OX063) or nitroxide-based 2,2,6,6-tetramethylpiperidine N-oxide (TEMPO) [34] with microwave irradiation. Dynamic nuclear polarization (DNP) [35,36] transfers polarization from electrons to nuclei upon microwave irradiation at or near the electron Larmor frequency.

Table 1
Overview of advantages and disadvantages of approaches to increase NMR sensitivity in solution.

Method	Absolute value of percent polarization $P_{\%}$	Advantages	Disadvantages
Optical pumping	Up to 90% ^a (^{129}Xe) [115,118]	<ul style="list-style-type: none"> High ^{129}Xe polarization values ^{129}Xe is chemically inert and very sensitive to chemical environment ^{129}Xe is soluble in water and biological fluids (e.g. liver, brain, blood) Excellent tool as a biosensor to detect the presence of a target molecule 	<ul style="list-style-type: none"> Application to protein studies in solution is mostly limited to Xe-binding proteins or engineered biosensors due to the low solubility of ^{129}Xe in water Detection is mostly limited to ^{129}Xe NMR Direct detection of protein resonances by SPINOE is modest to date
Dissolution DNP	Up to 40% ^b (^{13}C) [37,51]	<ul style="list-style-type: none"> High polarization can be achieved for low-γ nuclei Several biologically relevant molecules and different nuclei have been tested 	<ul style="list-style-type: none"> Biomolecules often do not respond well to the fast thawing process Significant sample dilution upon thawing Usually only one polarization step is possible due to large dilution upon thawing Long prepolarization times (min-hrs) are often necessary Due to fast T_1 relaxation, only a few transients can be acquired
Overhauser DNP	Up to 0.26% (^1H) [71]	<ul style="list-style-type: none"> Direct polarization in liquid phase Useful to study water dynamics 	<ul style="list-style-type: none"> Lower enhancements at high field Sample heating Current applications are confined to water and small molecules
Photo-CIDNP	Up to 0.23% (^1H , ^{15}N , ^{13}C , amino acids, peptides and proteins) [95]	<ul style="list-style-type: none"> Direct polarization in liquid phase Applicable to free amino acids, peptides, proteins and nucleic acids Wide range of sample concentration can be used ($\geq 5 \mu\text{M}$) Tri-enzyme additive prevents sample photodegradation and promotes dye recycling, supporting long-term data collection and 2D NMR Observed enhancements increase with laser power Very quick polarization buildup times (~ 0.1 s) 	<ul style="list-style-type: none"> Relatively small enhancements Only solvent-exposed aromatic amino acids undergo photo-CIDNP Samples eventually degrade after long exposure to high-power lasers
PHIP	<p>$\sim 100\%$ (^1H, hydrogenative PHIP) [105]</p> <p>$\sim 11.5\%$ (^1H, non-hydrogenative SABRE PHIP) [108]</p>	<ul style="list-style-type: none"> High polarization values Effective at low sample concentrations ($\sim \text{pmol}$) SABRE approach can be applied to a variety of molecules 	<ul style="list-style-type: none"> SABRE works only at $\sim \text{mT}$ magnetic fields Current applications are mostly confined to small molecules

^a Reported values refer to ^{129}Xe polarization achieved in the gas phase.

^b Reported values refer to polarization achieved after transfer to the liquid phase.

The sample is then rapidly melted and dissolved in a suitable hot solvent. The dissolved hyperpolarized sample is then rapidly transferred to a conventional liquid-state NMR setup for detection (Fig. 2A) [37,38].

Ardenkjær-Larsen, Golman and coworkers first examined the polarization of ^{13}C -urea in glycerol with OX063 as a trityl radical (15 mM, at 1.1 K, 94 GHz and 100 mW microwave source). They achieved a ^{13}C polarization up to 42% with a build-up time constant $\tau_{\text{DNP}} = 4900$ s in the solid state. Hot water was then rapidly injected into the sample, and the liquid mixture was then transferred within 6 s to a 9.4 T NMR magnet for detection. A remarkable fraction of the original ^{13}C polarization was preserved, with a net ^{13}C polarization of 37% observed after dissolution. After the hyperpolarization build-up time, this amounts to a ^{13}C S/N that is 44,400-fold larger than that of a reference ^{13}C NMR experiment conducted at 9.4 T and at room temperature in the absence of prior hyperpolarization (Fig. 2B and C) [37].

In solids, DNP is known to occur via a number of mechanisms known as the solid effect, thermal mixing and the cross effect [36]. The dependence of the observed polarization on microwave frequency led the authors to propose thermal mixing as the operating DNP mechanism, though contributions from solid effect could not be ruled out [37,38].

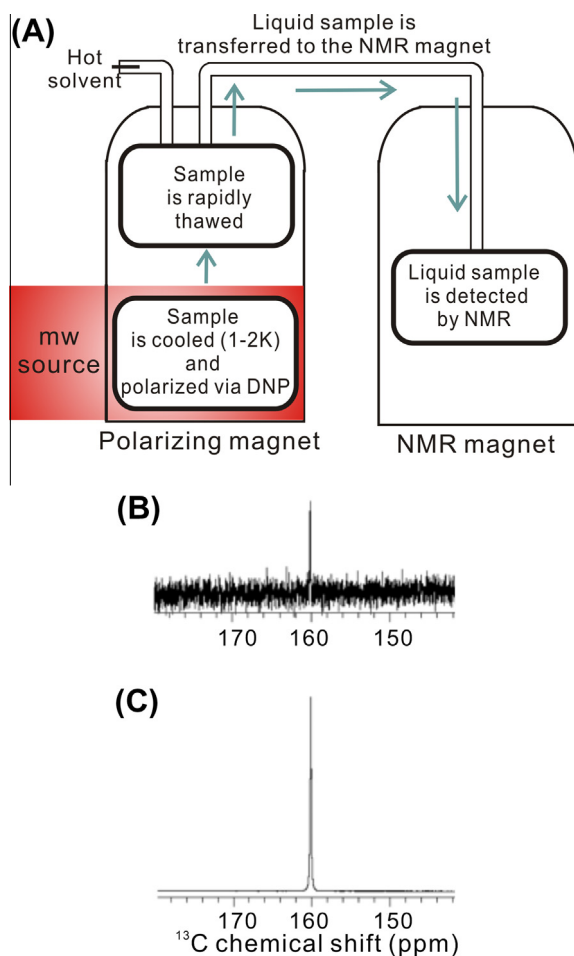


Fig. 2. (A) Schematic diagram illustrating the basic features of a dissolution DNP experiment. After hyperpolarization at low temperature by microwave (mw) irradiation, the sample is rapidly thawed and transferred to an NMR magnet for detection. (B) Reference ^{13}C NMR spectrum of liquid urea (natural isotopic abundance, 59.6 mM, 232,128 scans) with no prior hyperpolarization and data collection under Ernst-angle conditions. (C) ^{13}C NMR spectrum of liquid hyperpolarized urea (natural isotopic abundance, final concentration 59.6 mM, 1 scan) obtained via dissolution DNP in a 9.4 T NMR magnet with final $P_{^{13}\text{C}} = 20\%$. (Panels B and C were reprinted from Ref. [37].)

3.2. Relaxation and voyage times

The T_1 relaxation rate of the hyperpolarized nuclei is crucial in dissolution DNP. To preserve the nuclear polarization acquired in the solid state, polarized samples need to be thawed and transferred to the NMR spectrometer faster than the nuclear T_1 relaxation time [37]. Typical dissolution DNP samples experience a 'voyage time' as they are transferred from the polarizing magnet to the liquid state NMR magnet. During the voyage time, the sample is exposed to low fields (outside the magnets) of the order of 0.5 mT. T_1 is shorter at low field and even more so in the presence of the paramagnetic polarizing agent. Hence, short and fast voyages as well as removal of the stable free radical are crucial to minimize polarization losses [39].

Addition of the radical scavenger sodium ascorbate during the dissolution step alleviates polarization decays during and after the transfer. This process leads to a ~ 2 -fold extension of the ^{13}C T_1 of acetate (from 40.1 to 72 s) [40]. Attempts to shorten the voyage time included building a special spectrometer consisting of a single dual-isocentre superconducting magnet with 3.35 and 9.4 T polarizing and NMR-dedicated regions, respectively, separated by 83 cm. This system allows transferring the polarized sample to the NMR detection region within 2.9 s, i.e., ca. half of the time taken by conventional dissolution DNP systems [41].

In systems with nuclear spin states delocalized over two or more spins, long-lived nuclear spin states can be generated [42–45]. Now, the intramolecular dipole–dipole interaction is symmetric with respect to spin exchange, while the singlet and triplet spin states are antisymmetric and symmetric, respectively. Therefore, the dipole–dipole interaction cannot mediate symmetry-breaking singlet-to-triplet transitions [46]. While triplet states are able to relax via intramolecular dipole–dipole interactions within the triplet manifold, singlet nuclear spin states are unable to undergo intramolecular dipole–dipole relaxation and display remarkably long T_1 values, typically ranging between a few tens of seconds and several minutes [46,47]. Methods relying on this property were able to generate long-lived singlet spin states in the context of dissolution DNP, and thus improve the effectiveness of this approach. For instance, the lifetimes of the Ala-Gly dipeptide H^α protons were increased by 7-fold (over the regular T_1) [47], rendering this peptide suitable for dissolution DNP.

3.3. Hyperpolarizing agents

In addition to the TEMPO-like or trityl radicals, alternative hyperpolarizing agents like 1,3-bisdiphenylene-2-phenylallyl (BDPA) have recently been proposed [48]. Hyperpolarized $[1-^{13}\text{C}]$ pyruvic acid in sulfolane yielded a 14,000 ($P_{^{13}\text{C}} = 11\%$) and 12,000 ($P_{^{13}\text{C}} = 9.7\%$) sensitivity enhancement (298 K, $B_0 = 9.4\text{T}$) in the presence of BDPA and trityl OX063, respectively. The polarization build-up time was not taken into account when computing sensitivities. Unlike trityl radicals, BDPA is water-insoluble. Hence it can be conveniently removed from the hyperpolarized solution by filtration during the dissolution step.

3.4. Cross-polarization enhancement of low- γ nuclei

High- γ nuclei like ^1H polarize fast and efficiently, yet have short T_1 , hence they tend to depolarize fast during transfer to the NMR magnet. Jannin et al. carried out experiments showing that cross polarization (CP) from ^1H to ^{13}C leads to rapid and significant increase in ^{13}C polarization under typical dissolution DNP conditions [49]. Batel et al. went further and showed that, after CP in the solid state, ^{13}C polarization is mostly preserved upon dissolution and detection [50]. These researchers employed 4.5 M ^{13}C -urea doped with 30 mM TEMPO. The sample was first hyperpolarized (build-

up time constants: $\tau_{1H} = 580$ s and $\tau_{13C} = 1014$ s) followed by CP, which doubled ^{13}C polarization, ending up with a final solid-state polarization of 14% achieved within half of the regular build-up time. The ^{13}C polarization after dissolution was retained to a significant level (8.8%). Even higher ^{13}C polarization levels ($P_{\%,13C} \approx 45\%$ in the solid state and $P_{\%,13C} \approx 40\%$ in solution at 300 K) were achieved by performing CP at the higher polarizing field of 6.7 T [51].

3.5. Additional hyperpolarization enhancers

Addition of lanthanide ions like gadolinium (Gd^{3+}) and holmium (Ho^{3+}) was shown to further enhance the ^{13}C polarization of pyruvate in the solid state. Unfortunately, lanthanides also reduce ^{13}C T_1 values in the liquid state, preventing the use of this strategy in dissolution DNP. However, it was recently shown that addition of chelating agents such as diethylenetriamine pentaacetate (DTPA) during the dissolution process drastically reduces the liquid-state relaxivity of Gd^{3+} , thus minimizing liquid-state relaxation [52]. Hence this method is potentially useful for further increases in NMR sensitivity by dissolution DNP.

3.6. 2D experiments

An unavoidable drawback of dissolution DNP is the inability to perform iterative DNP, freeze–thaw and transfer steps, limiting multidimensional NMR applications.

Yet, a variety of methods to collect 2D NMR data have recently been developed. These include small-tip-angle excitation [53], spatially encoded ultrafast 2D NMR [54], scaling of heteronuclear coupling by optimal tracking (SHOT) [55], hyper single-point amplitude-separated multi-dimensional (SPASM) NMR [56] and hyperpolarized Hadamard spectroscopy [57].

3.7. In situ temperature-jump DNP

Griffin et al. developed an alternative approach to hyperpolarize samples in the liquid state. The sample is frozen at 90 K and ^1H is polarized with a biradical polarizing agent (5 T, 140 GHz microwave source). Polarization is then transferred to low- γ spins via cross polarization. The sample is then melted by irradiation with an infrared pulsed laser, followed by NMR detection (with ^1H decoupling) within the same device. An advantage of this method is that it enables iterative hyperpolarization cycles, given that sample melting and NMR spectroscopy are performed *in situ*. Therefore, the entire cycle can be repeated and signal averaging can be performed [58].

3.8. Additional applications

Extensive dissolution DNP investigations have been carried out to probe the metabolic activity of tissues (e.g. heart, liver, tumor cells) [38]. For instance, hyperpolarized $[1-^{13}\text{C}]\text{pyruvate}$ is used as a clinical diagnostic tool in metabolic imaging to characterize differences between normal and tumorigenic cells [59]. Additional applications of more biophysical nature include real-time enzyme kinetics [60], studies of biosynthetic pathways [60], detection of poorly-populated reaction intermediates [61], and ligand-detected protein–ligand interactions [62]. Recently, the pH-jump-induced refolding of the hyperpolarized ribosomal protein L23 was studied in real time by monitoring the time course of the ^{13}C NMR signal intensities [63].

4. Overhauser dynamic nuclear polarization

Unlike the dramatic polarization enhancements achieved in solid-state DNP, which are close to the theoretical limit, smaller enhancements are typically observed in liquid-state Overhauser DNP. Here we briefly review the origin of the Overhauser DNP enhancement (Fig. 3A and B), recent efforts to increase them, and some representative applications.

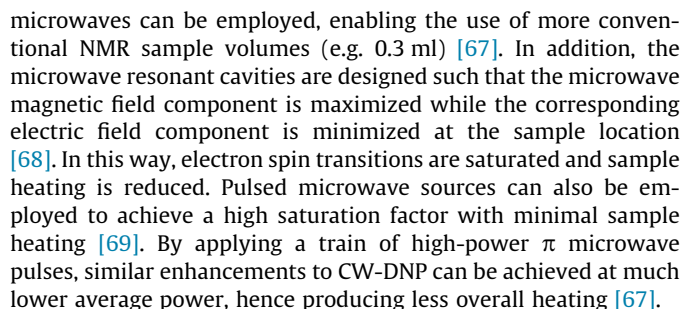
Polarization transfer can occur in solution via the well-known Overhauser effect, which was first observed by Albert Overhauser in 1953 [35] and proceeds via dipolar and scalar interactions between an unpaired electrons and a nearby NMR-active nucleus [64]. The Overhauser enhancement factor, which expresses the enhancement of nuclear polarization in the presence of nearby saturated electrons, is expressed as [64]

$$\varepsilon = \frac{\langle I_z \rangle - I_{eq}}{I_{eq}} = \xi f s \frac{\gamma_e}{\gamma_n}, \quad (6)$$

where $\langle I_z \rangle$ is the longitudinal magnetization, I_{eq} is the equilibrium magnetization, ξ is the coupling factor, f is the leakage factor, s is the saturation factor, γ_e is the gyromagnetic ratio of the electron, and γ_n is the gyromagnetic ratio of the nucleus. The coupling factor (ξ) represents the efficiency of electron–nucleus cross-relaxation, the leakage factor (f) describes the portion of nuclear relaxation due to the electron, and the saturation factor (s) reflects the efficiency of microwave pumping. The main challenges to the study of biomolecules via Overhauser DNP are discussed below. First, the coupling factor ξ decreases with magnetic field and molecular size in liquids, where the dipolar contribution to ξ dominates over the scalar contribution [64,65]. Second, high-power microwave irradiation is necessary to achieve high saturation factors, and this often results in sample heating, especially at high polarizing fields. Third, performing the experiment at physiologically relevant temperatures limits the maximum achievable electron and nuclear polarization to a few percent even with modern superconducting magnets as shown in Eq. (3) and discussed by Günther [38].

Regardless of the initially prepared nuclear polarization, the NMR S/N increases with B_0 , as shown in Eq. (5). In addition, spectral resolution increases at high field [3]. Thus, high fields are generally desirable in liquid-state NMR. Therefore, a major challenge of Overhauser DNP as an NMR sensitivity-enhancement tool is the decrease in coupling factor ξ at high applied fields. Specifically, ξ is proportional to B_0^{-2} for rotational-diffusion-mediated relaxation, and to $B_0^{-3/2}$ for translational-diffusion-mediated relaxation. The coupling factor ξ becomes proportional to B_0^{-1} in molecular dynamics (MD) simulations that take into account the complex solute–solvent dynamics at atomic detail over a wide range of timescales [66]. Computational predictions on the field dependence of ξ via MD simulations agree well with experimental results [67], as illustrated in Fig. 3C. This figure also shows good agreement between experimental data and theoretical predictions obtained from a force-free model. In both cases, translational and rotational correlation times from experimental NMR relaxation dispersion measurements were employed as input parameters.

To overcome the unfavorable magnetic field dependence, shuttle-DNP spectrometers (Fig. 3A) have recently been developed so that nuclei are first polarized by microwave irradiation upon saturation of the EPR transitions at low magnetic field, followed by sample or probe transfer to high field for detection [67]. Note, however, that since initial nuclear polarization increases with applied magnetic field, larger net nuclear polarization can be observed at high fields despite the relatively small coupling and enhancement factors. The use of pulsed microwave sources for coherent polarization transfer provides another potential avenue to overcome the unfavorable field dependence of DNP polarization [67].



In liquids, the Overhauser DNP enhancement decreases in the presence of slow molecular diffusion (i.e., when translational correlation times are larger than \sim ns), posing challenges to the application of liquid-state Overhauser DNP to large molecules of biological interest [64,65]. For instance, when the diffusion of water is slow, a dramatic decrease in water DNP efficiency is observed [70]. The feasibility of studying ubiquitin or even larger biomolecules has been proposed [67], based on the shuttle-DNP polarization of the fast-rotating methyl groups, whose importance in NMR macromolecular characterization has been established [27].

Water is one of the most popular Overhauser DNP substrates since it gives high DNP polarization enhancements due to its fast rotational and translational diffusion. The absolute value of the water ^1H polarization reaches 0.26% at 260 GHz microwave irradiation in a 9.2 T magnet (in high-field DNP experiments) in the presence of the ^{14}N -TEMPOL nitroxide radical (1 M) at 160 °C (Fig. 3D) [71]. This high temperature results from sample heating at high microwave power. On the other hand, 0.04% was obtained for the absolute value of the Overhauser DNP polarization at 45 °C [71], in the presence of lower-power microwave irradiation. The high Overhauser DNP enhancement of small molecules, including water, has been exploited in many applications. For instance, polarization-enhanced water has served as MRI contrast agent [72], and water dynamics has been site-specifically probed near proteins (e.g., myoglobin) in different folding states [70] and in the vicinity of lipid membranes [73] and membrane-protein interfaces [74].

In 1967, a surprising case of NMR-detected nuclear polarization induced by a chemical reaction was originally observed in organic polymerizations promoted by free radical initiators [75] and in halogen-metal exchange processes [76]. Soon thereafter it was discovered that nuclear polarization could also be generated upon photo-excitation of a redox-competent dye in the presence of a biomolecule of interest [77]. This phenomenon, known as photochemically induced dynamic nuclear polarization (photo-CIDNP), has mainly been exploited to study processes such as protein folding and biomolecular interactions, which involve variations in the solvent exposure of specific amino acids since the photo-CIDNP mechanism involves the direct interaction between the photo-excited dye and the substrate of interest [78,79]. Recent developments, however, have begun to explore the photo-CIDNP effect for NMR sensitivity enhancement purposes in liquid solutions containing biological molecules.

A typical photo-CIDNP sample contains a biomolecule of interest in a liquid solution in the presence of a photoexcitable dye, such as flavin mononucleotide (FMN) or 2,2'-dipyridyl. Sample photo-irradiation (e.g. by an argon ion or a frequency-tripled Nd:YAG laser) directly in the NMR spectrometer may be facilitated by routing the light to the NMR sample tube via an optical fiber (Fig. 4A) [80,81]. Pulse sequences can be designed to control the relative timing of both the UV-VIS irradiation (to generate

Another concern in Overhauser DNP is sample heating due to microwave irradiation. This issue is particularly relevant when irradiation is performed at high magnetic field, where the limited penetration depth necessarily confines sample volumes to a few nanoliters [67]. The shuttle-DNP approach helps overcoming this challenge since at low polarizing field relatively low-frequency

photo-CIDNP polarization) and the radio-frequency pulses (to perform the NMR experiment). Present implementations of photo-CIDNP enhance the polarization of nuclei belonging primarily to the Trp, His and Tyr amino acids and all nucleotide bases [79]. Other molecules can potentially be photo-CIDNP-active as long as they (a) are capable of being transiently oxidized by the photoexcited dye and (b) give rise to a radical cation whose EPR g factor bears an appropriate difference with the g factor of the transiently reduced radical anion dye [79].

According to the radical pair mechanism of photo-CIDNP [82,83], the dye is photoexcited to generate a long-lived (μs – ms) triplet state. Upon encounter of the triplet excited dye with the molecule of interest, one electron (or H^\bullet) is transiently transferred from the target molecule to the dye, giving rise to a triplet radical pair (Fig. 4B). This radical pair then undergoes either one of two pathways, depending on the nuclear spin state of the molecule of interest.

In the first-case scenario, i.e., when the molecule of interest is in its α nuclear spin state, the radical pair may undergo fast triplet-to-singlet intersystem crossing (TS-ISC). Then, TS-ISC followed by recombination via back-electron transfer produces the original target molecule with spin preservation in the α state (Fig. 4B). We denote this process as the recombination route. Note that only a singlet radical pair is allowed to undergo recombination.

Alternatively, i.e., when the molecule of interest is in its β nuclear spin state, the radical pair may undergo a slower TS-ISC. Then the ion pair is more likely to dissociate before undergoing TS-ISC, and the target molecule would undergo paramagnetic nuclear relaxation to produce comparable populations of α and β spins (Fig. 4B). We denote this process as the escape route. Note that the specific route followed by the α and β spins switches, when the sign of either the hyperfine coupling constant A or Δg changes (see Eq. (10)). Importantly, the actual difference between the TS-ISC rates of the α and β spins determines the relative flux through the recombination and escape routes and is, in turn, proportional to the extent of photo-CIDNP.

At a more quantitative level, the TS ISC rate (ω_{TS}) can be expressed as [79,84]

$$\omega_{\text{TS}} = |\omega_M - \omega_D|, \quad (7)$$

where ω_M and ω_D are the unpaired electron EPR precession frequencies of the radical cation state of the target molecule M^+ and the radical anion state of the dye D^- , respectively. In the simple case of a target molecule carrying only one NMR-active spin $1/2$ nucleus, we have

$$\omega_M = g_M \mu_B B_0 / \hbar \pm A/2 \quad \text{and} \quad \omega_D = g_D \mu_B B_0 / \hbar, \quad (8)$$

where g_M and g_D are the g factors of M^+ and D^- , respectively, μ_B is the Bohr magneton, B_0 is the applied magnetic field, and A is the hyperfine coupling constant between the unpaired electron and the unique NMR-active nucleus in M^+ . The $+$ and $-$ signs apply to the α and β nuclear spin states, respectively. It follows from Eq. (7) and (8) that, for radical pairs containing a spin $1/2$ nucleus, the TS-ISC rate is

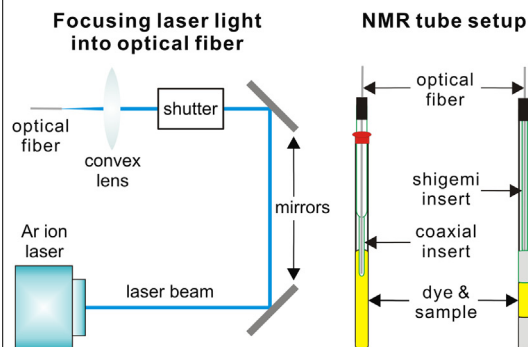
$$\omega_{\text{TS}} = \Delta g \mu_B B_0 / \hbar \pm A/2, \quad (9)$$

where Δg is the difference between the g factors of M^+ and D^- . The TS-ISC probability for the α and β spins is given by

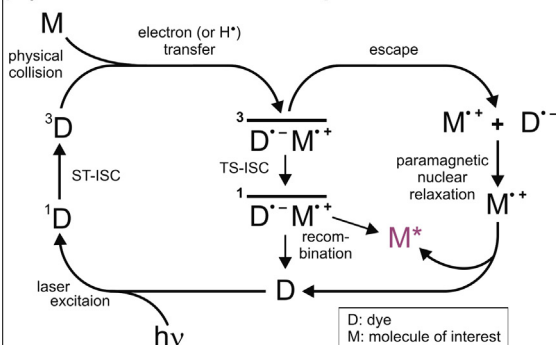
$$P_{\text{TS},\alpha} = \sin^2 \frac{\omega_{\text{TS},\alpha}}{2} t = \sin^2 \left(\frac{\Delta g \cdot \mu_B B_0}{2\hbar} + \frac{A}{4} \right) t$$

$$P_{\text{TS},\beta} = \sin^2 \frac{\omega_{\text{TS},\beta}}{2} t = \sin^2 \left(\frac{\Delta g \cdot \mu_B B_0}{2\hbar} - \frac{A}{4} \right) t. \quad (10)$$

(A) Photo-CIDNP instrument setup



(B) Photo-CIDNP radical pair mechanism



(C) Photo-CIDNP spectra

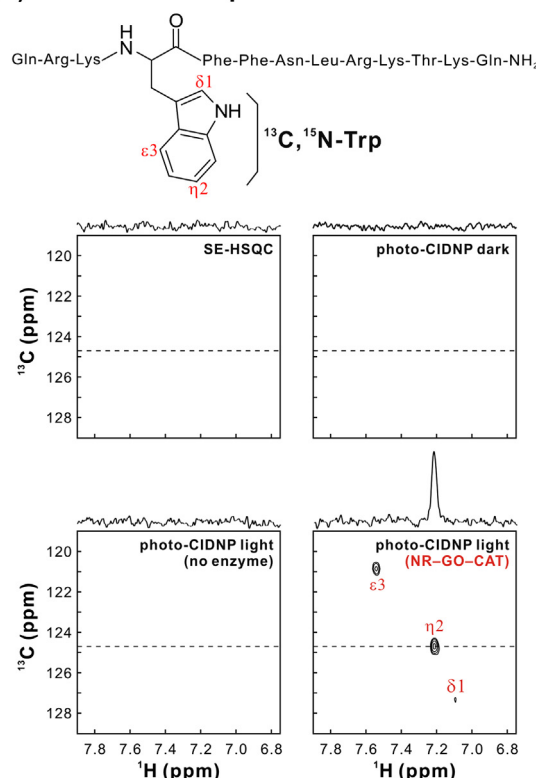


Fig. 4. Overview of photo-CIDNP. (A) Instrumental setup. (B) Radical pair mechanism of photo-CIDNP in liquids. M^\bullet denotes the spin-polarized molecule of interest. (C) 2D ^{13}C -PRINT photo-CIDNP spectra of the σ^{32} peptide (13-amino acids, 20 μM , 600 MHz spectrometer) in the absence and presence of catalytic amounts of the photo-CIDNP-enhancing NR-GO-CAT tri-enzyme system [95]. (Reprinted from [95].)

The photo-CIDNP signal intensity increases with $|p_{TS,\alpha} - p_{TS,\beta}|$. Hence, as evident from the above relation, the efficiency of photo-CIDNP depends critically on the hyperfine coupling constant A , the applied field, and the Δg value, in addition to other factors including the redox properties of the dye, the molecule of interest and the accessibility of the molecule of interest to physical collision with the dye.

The effect of magnetic field strength on photo-CIDNP is highlighted by the following experiments [85–87]. The applied magnetic field was varied between 0 and 7 T to monitor His, Tyr and Trp photo-CIDNP in the presence of the 2,2'-dipyridyl dye. For Tyr, His and Trp the maximum net photo-CIDNP (longitudinal one-spin order) was observed at ca. 2, 7 and >7 T, respectively. The origin of the observed variation in maximum photo-CIDNP response is likely due to the g factor difference between amino acid and dye.

As previously mentioned, photo-CIDNP has recently become a promising NMR sensitivity enhancement tool. ^1H CIDNP and ^1H CIDNP followed by ^1H - ^{15}N HSQC (*light*) on Trp indole NH were shown to provide ~6.5-fold higher enhancement than corresponding *dark* experiments acquired in the absence of laser irradiation [88]. This result corresponds to a ~0.03% ^1H polarization, assuming that resonance intensity is proportional to polarization. Photo-CIDNP-enhanced versions of the ^1H - ^{15}N HMQC and SOFAST-HMQC pulse sequences were also developed [89].

As originally shown by Hore and coworkers [88], ^{15}N photo-CIDNP followed by ^1H detection provides another convenient route to enhance NMR sensitivity. This approach exploits the high hyperfine coupling between the Trp unpaired electron and the indole nitrogen together with the sensitivity of ^1H NMR to provide 100-fold higher sensitivity than a reference dark experiment. While this effect corresponds to only a moderate ~0.05% ^{15}N polarization, it leads to a ~10-fold higher sensitivity than a reference pulse-field-gradient sensitivity-enhanced ^1H - ^{15}N HSQC experiment. In addition, advanced pulse schemes exploiting both ^1H and ^{15}N photo-CIDNP in the context of ^1H -detected heteronuclear correlation have also been developed [90].

The high ^{13}C hyperfine coupling constants and the presence of several CH bonds in aromatic amino acids led to the development of ^1H -detected ^{13}C CIDNP in the context of heteronuclear correlation spectroscopy [91]. Up to 16-fold higher sensitivity than a reference sensitivity-enhanced HSQC was achieved, corresponding to ~0.08% ^{13}C polarization. Several CH bonds of Trp, Tyr and Trp were enhanced in this experiment, including ^{13}C bonds.

In addition to the high photo-CIDNP effect of the ^{13}C and ^{15}N heteronuclei, engineering amino acids containing other heteronuclei with potentially high hyperfine coupling constants provides another route to enhance photo-CIDNP sensitivity. For instance, up to 40-fold sensitivity enhancement (~0.18% polarization) was observed for the ^{19}F nucleus (in the 3-fluorotyrosine – FMN pair), which has a high gyromagnetic ratio and a high hyperfine coupling constant upon transient 3-fluorotyrosine oxidation [92].

One major advantage of photo-CIDNP is that it can be performed under mild solution conditions, given that no freeze–thaw cycles or extrinsic stable radicals are required. This feature enables multiple transients to be collected within short time spans, providing the opportunity to increase S/N by signal averaging and/or acquire multidimensional photo-CIDNP data. In practice, however, dye photoreduction (typically FMN to FMNH₂) and sample photodegradation mediated by singlet oxygen impose severe limitations on sample integrity and prevent prolonged photo-CIDNP data collection.

In order to promote the necessary reoxidation of FMNH₂ to FMN, two strategies have been employed. First, mechanical mixing of the NMR sample between scans served to facilitate oxidation of FMNH₂ by ambient oxygen [93]. Alternatively, hydrogen peroxide

was added to the sample as an FMNH₂ oxidant [93]. In addition, the effect oxygen level on photo-CIDNP was monitored [94]. Saturation of ambient oxygen to facilitate FMNH₂ reoxidation caused quenching of triplet-excited dyes, eliminating photo-CIDNP. Likewise, depletion of ambient oxygen to prevent O₂-dependent sample photodegradation caused inefficient reoxidation of FMNH₂. More recently, simultaneous prevention of sample photodegradation and dye photoreduction has been achieved by the development of a tailored additive known as the NR-GO-CAT tri-enzyme system [95]. This trio of commercially available enzymes, added to NMR samples in minute catalytic amounts, prevents oxygen-mediated sample degradation and facilitates the efficient and specific reoxidation of FMNH₂ in photo-CIDNP experiments. This strategy enabled prolonged photo-CIDNP on amino acids, the σ^{32} peptide and the drkN SH3 protein at micromolar concentrations, and led to 48-fold greater NMR sensitivity than the reference HSQC experiment.

The latter experiment leads to ~0.23% ^{13}C polarization, corresponding to a ~190-fold ^{13}C polarization enhancement relative to the Boltzmann distribution. This result paves the way to long-term photo-CIDNP data collection, which was impossible before. Thanks to the tri-enzyme system, the photo-CIDNP polarization enhancement is achieved iteratively within an experiment, and complex biomolecules can be analyzed in solution at low micromolar concentrations.

Photo-CIDNP experiments at low magnetic field directly (de)populate singlet nuclear spin states of His βH 's with long-lived (ca. 1 min) longitudinal magnetization, suggesting promising *in vivo* applications [96].

A pulse sequence for iteratively accumulating photo-CIDNP within a spin system before readout was developed [97]. This strategy is helpful when periodic pulsed laser light sources are employed. Finally, a remarkable ~4% ^{13}C polarization, corresponding to a ~10,000-fold ^{13}C NMR sensitivity enhancement, was recently achieved via photo-CIDNP for a bacterial photosynthetic reaction center [98]. The high polarization, which is currently the highest achieved via photo-CIDNP in liquids and is specific to this system, stems from the persistence of large anisotropic components in the hyperfine coupling, within the electron-donor chlorophyll radical. Three photo-CIDNP mechanisms, denoted as three-spin mixing, differential decay and differential relaxation were shown to prevail when the electron donor and acceptor members of the radical pair tumble very slowly and are at a nearly invariant relative distance and orientation [99,100].

6. Parahydrogen-induced polarization

Molecular hydrogen comes in two isomers, ortho and para, which have symmetric (triplet) and antisymmetric (singlet) nuclear spin states, respectively. The ortho and para isomers are populated as a 3:1 ratio at room temperature, with the ortho isomer being more populated [101]. Interconversion between the two isomers is symmetry forbidden and occurs very slowly. Thus, when hydrogen is flowed through an appropriate paramagnetic catalyst, especially at low temperature (~20 K) where parahydrogen is much more stable than orthohydrogen, close to 100% parahydrogen population can be achieved and exploited at ambient temperature [102]. In para-hydrogen-induced polarization (PHIP), nuclear polarization is attained by transferring the high spin order of parahydrogen to the molecule of interest [101] (Fig. 5A).

Typically, PHIP applications involve the direct incorporation of parahydrogen into unsaturated organic molecules via hydrogenation. The new chemical environment experienced by the two protons upon hydrogenation breaks the singlet symmetry and renders the spin system detectable by NMR. Depending on whether

hydrogenation is carried out at high or low magnetic field (followed by sample transfer and detection at high magnetic field), the PHIP methods are known as PASADENA [103] or ALTADENA [104], respectively (Fig. 5A). In PASADENA (Parahydrogen and Synthesis Allow Dramatically Enhanced Nuclear Alignment), the parahydrogen singlet symmetry is immediately broken upon hydrogenation due to the distinct chemical shift environment of the two incorporated protons at high magnetic field, and the singlet $\frac{1}{\sqrt{2}}(|\alpha\beta\rangle - |\beta\alpha\rangle)$ parahydrogen is collapsed into two eigenstates, $|\alpha\beta\rangle$ and $|\beta\alpha\rangle$. Thus the NMR spectrum shows two antiphase multiplets. In ALTADENA (Adiabatic Longitudinal Transport after Dissociation Engenders Net Alignment), since the chemical shifts are essentially the same when parahydrogen is incorporated into the substrate at low magnetic field, the singlet state becomes selectively polarized as $|\alpha\beta\rangle$ or $|\beta\alpha\rangle$ upon adiabatic transfer to high magnetic field. In this case the NMR spectrum is characterized by two hyperpolarized resonances of opposite sign. In case there are other nuclei in the substrate, NOE, scalar and dipolar coupling can cause spin order to spread throughout the substrate during the initial low-field step [101]. Nuclear polarizations of $\sim 100\%$ were observed [105] and 0.1 μM concentrations of pyridine [106] were monitored via inorganic-complex-based PHIP.

Despite the high polarization achieved by PHIP, the method is not generally applicable to biomolecules due to the necessary covalent sample modifications. Recently, a very interesting related methodology known as Signal Amplification by Reversible Exchange (SABRE, or Non-Hydrogenative Parahydrogen-Induced Polarization; NH-PHIP; Fig. 5) [107] was developed to polarize substrates in the absence of hydrogenation. In the SABRE experiment, substrate and parahydrogen establish transient contacts via a metal center. While the complex is formed, nuclear polarization is transferred from the ^1H nuclei derived from parahydrogen to the molecule of interest. After the polarization transfer, the highly polarized intact substrate is released. Pyridine has been the most popular substrate for SABRE and up to $\sim 11.5\%$ ^1H polarization has been achieved [108]. Remarkably, SABRE shows promise to extend its substrate to other small molecules including short polypeptides [109].

The SABRE approach is similar to ALTADENA in that polarization by parahydrogen occurs at low magnetic field. Interestingly, the magnetic field dependence of the SABRE signal changes very little with substrate type or proton position [110]. This result is in line with the theoretical prediction that the extent of polarization depends primarily on the scalar coupling between two parahydrogen-derived protons but not on the scalar coupling between parahydrogen-derived and substrate protons, within the metal complex [111]. Unlike ALTADENA, however, SABRE does not necessarily involve adiabatic sample transfer to high magnetic field for detection, and optical atomic magnetometer or SQUID devices can be employed for detection even at low magnetic fields [112].

7. Optical pumping

Optical pumping utilizes the ability of circularly polarized light to selectively excite a specific quantum state of an alkali metal, typically Rubidium (Rb). Excellent reviews are available on this topic [113] and we will limit our survey to the basic principles and most exciting applications relevant to the quest for high NMR sensitivity within the biological context. For instance [113], if right (with respect to an external magnetic field) circularly polarized light σ^+ is applied to the $^2S_{1/2}$ ground state of Rb vapor, the Rb atoms carrying a total electron azimuthal angular momentum quantum number $m_j = -1/2$ are selectively excited to the $^2P_{1/2}$

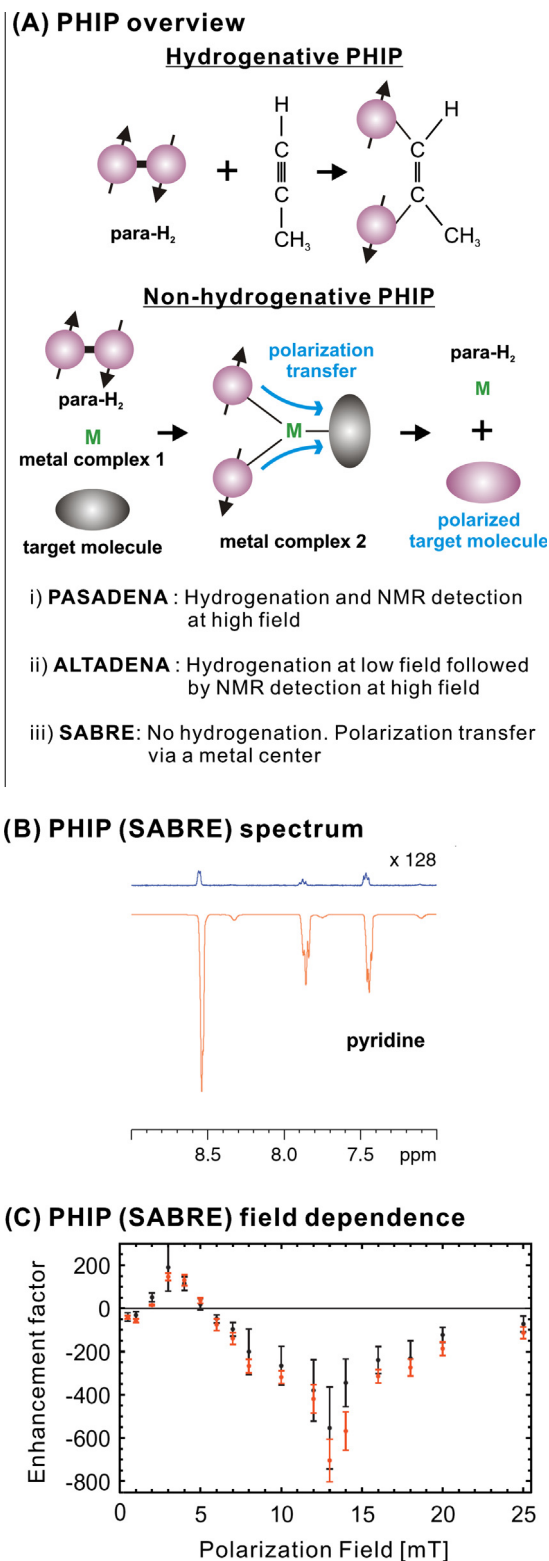


Fig. 5. Schematic representation of PHIP. (A) Overall mechanistic schemes for hydrogenative and non-hydrogenative PHIP. (B) Non-hyperpolarized control (top) and SABRE-polarized (bottom) ^1H spectra of 6 nmol of pyridine [107]. The top spectrum is a 128-fold vertical expansion of the bottom spectrum. (Reprinted from [107].) (C) Magnetic-field dependence of the SABRE PHIP enhancement factor for the proton linked to the pyridine C_4 . Black and red dots denote regular pyridine and a 10:1 mixture of deuterated/protonated pyridine, respectively. Enhancement factors denote the ratio between the polarized and unpolarized signals. (Reprinted from [110].)

state with $m_j = +1/2$. Note that this discussion neglects the Rb electron-nucleus hyperfine coupling, for simplicity. The above photo-excitation process is usually carried out in a N_2 gas atmosphere to promote nonradiative relaxation and prevent deleterious radiation trapping [113,114]. Indeed, collision of gaseous N_2 with the excited alkali-metal promotes nonradiative conversion to the $^2S_{1/2}$ ground states that have either $m_j = +1/2$ or $m_j = -1/2$. Because the right polarized light is unable to excite $^2S_{1/2}$ Rb with $m_j = +1/2$, this state will not get depopulated. As a result of continuous light absorption and subsequent relaxation, including spontaneous emission and collision-induced nonradiative relaxation, a large number of atoms accumulate in the $^2S_{1/2}$ state with $m_j = +1/2$ (Fig. 6A).

After the above electron polarization step, spin-exchange between the polarized Rb and a noble gas takes place (Fig. 6B). This process is mediated by the hyperfine interaction, which enables the transfer of electron spin polarization of Rb to the nuclear spin of the noble gas [113]. As a result, enhanced nuclear spin polarization is observed for the noble gas. Polarizations greater than 50% (Fig. 6C and D) and about 80% have been reported for ^{129}Xe [115,116] and ^3He , respectively [117]. The polarization build-up time depends on experimental conditions. For instance, 7.5% of the xenon polarization is achieved in 5 min at 2.2 atm pressure [118].

^3He and ^{129}Xe are the most commonly used noble gases for spin-exchange optical pumping (SEOP). ^{129}Xe , whose natural abundance is 26%, is particularly useful in the context of biology because, in addition to its chemical inertness, it is highly polarizable due to its large electron cloud. Hence ^{129}Xe NMR is extremely sensitive to the surrounding environment and can be used at low concentrations, despite the moderately small value of this nucleus' gyromagnetic ratio (ca. 3.8 times smaller than ^1H) [119,120]. For instance, xenon dissolves in water up to 190 μM at 310 K and 0.058 atm partial pressure [121]. In addition, ^{129}Xe is one order of magnitude more soluble than ^3He in biologically relevant fluids such as water and blood at room temperature [122].

Among the numerous ^{129}Xe applications reported so far [123,124], those based on the spin-induced nuclear Overhauser effect (SPINOE) are particularly promising. SPINOE takes advantage of the cross-relaxation between hyperpolarized ^{129}Xe and neighboring ^1H spins to accomplish polarization transfer to the protons. Hence, this effect enhances NMR sensitivity for the detection of protons in solution [122,125]. SPINOE was used primarily to study organic molecules containing xenon-accessible cavities such as α -cyclodextrin and cryptophane-A [123] as well as in the context of proteins larger than 100 amino acids [126]. The hydrophobic cavity of the 10 kDa protein β -cryptogin was studied by SPINOE at 1.6 mM in the presence of 5.2 mM $\sim 15\%$ hyperpolarized xenon. A small but clearly distinguishable increase in ^1H resonance intensity (by $\sim 1\%$) was observed in the inner core of the protein [127]. Additional details about SPINOE can be found elsewhere [122].

Xenon has also been used as a biosensor so that the presence of certain molecules, rather than their conformational features, can be detected at high sensitivity. Xe-based molecular sensors consist of three parts: a cage containing hyperpolarized ^{129}Xe , a ligand head designed to bind the chosen target with high affinity, and a tether linking the above components. Binding of the ligand head to the target molecule is sensed via ^{129}Xe NMR chemical shifts, so that quantitative information on the amount of bound protein ligand can be gained [123,128]. One of the most commonly used cages is cryptophane-A, and various cryptophane derivatives as well as other potential cages (e.g., cucurbit[6]uril and cucurbit[5]uril derivatives) have also been explored [120,129].

To further increase NMR sensitivity, ^{129}Xe hyperpolarization and chemical exchange saturation transfer (CEST) were combined in Hyper-CEST [130]. The spin pool of Xe atoms encapsulated in

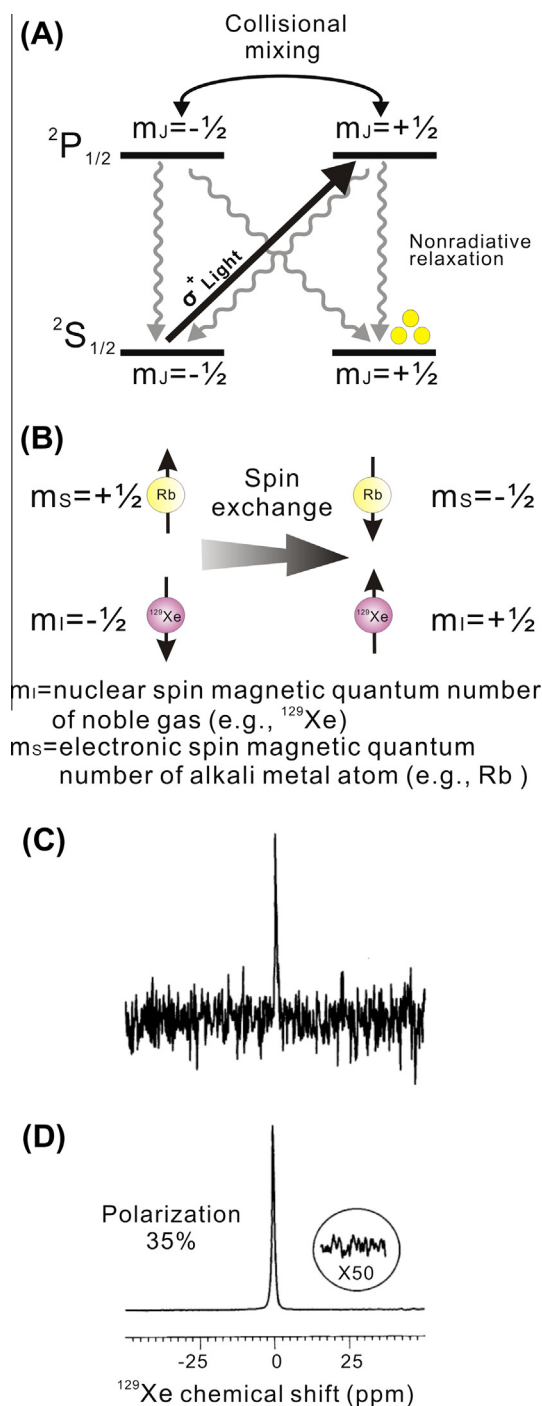


Fig. 6. Overview of Optical pumping. (A) Scheme illustrating the optical pumping of an alkali metal upon irradiation with right circularly polarized σ^+ light (the hyperfine coupling between electronic and nuclear spins is ignored). The process leads to an enriched population of the alkali metal in the $m_j = +1/2$ ground electronic state (yellow circles). (B) Polarization transfer via spin exchange between the electron spin of an alkali-metal atom (e.g. Rb) and the nuclear spin of a noble gas (e.g. ^{129}Xe). (C) Reference 1D ^{129}Xe NMR spectrum of 5×10^{19} gaseous Xe atoms in the absence of optical pumping. (D) 1D ^{129}Xe NMR spectrum of 2×10^{17} gaseous Xe atoms (1 scan) polarized by optical pumping ($P_{\%}^{129\text{Xe}} = 37\%$). (Panels C and D were reprinted from [155].)

the cage is saturated by frequency-selective radiofrequency pulses and transferred by chemical exchange to the larger free Xe spin pool in solution. This results in a decrease in signal by the free bulk hyperpolarized Xe. This effect is indicative of the presence of caged Xe, hence it reports on the presence of the target molecule.

A ^{129}Xe NMR experiment with direct (5%) Xe hyperpolarization provides $\sim 10^4$ higher sensitivity than a reference experiment with unpolarized Xe, disregarding the polarization build-up time. Hyper-CEST provides a further ~ 4000 -fold sensitivity enhancement relative to the direct-hyperpolarized Xe experiment [121]. Hence, hyper-CEST achieves an unprecedented overall increase in sensitivity by seven-orders of magnitude relative to the unpolarized Xe experiment, disregarding the Xe hyperpolarization build-up time [120]. Finally, a newly developed ^{129}Xe Hyper-CEST agent based on readily prepared perfluorocarbon (PFC) nanoemulsion droplets shows great promise for easily accessible future applications [131].

8. When sensitivity is not a top priority: rapid data collection schemes

In NMR applications monitoring kinetics in real time and in experiments that require high-dimensionality ($\geq 2\text{D}$), a reduction of the total experiment time can be critically important, even in the case of concentrated samples.

The total data collection time of multidimensional NMR experiments can be significantly shortened by a suite of approaches known as reduced sampling techniques. Hence, in terms of amount of useful data collected per unit time, reduced sampling techniques can be regarded as powerful tools. These approaches include non-uniform sampling (NUS) [132–135], knowledge-based optimized data undersampling [136], and non-Fourier methods like Hadamard spectroscopy [137].

Interestingly, some studies reported that, depending on the sampling strategy and reconstruction method, NUS may give rise to an actual increase in the S/N ratio and “detection sensitivity”, i.e., the probability of detecting weak peaks, compared to uniformly sampled experiments with an identical total data collection time [138]. However, it needs to be noted that NUS often involves reconstruction procedures that require cautious monitoring of the reliability of the output spectral features [139].

In addition, spatially encoded ultrafast nD NMR methods take advantage of parallel data collection in multiple regions of the sample in the presence of fast-switching pulse field gradients. Ultrafast nD NMR enables the acquisition of complete multidimensional NMR spectra within a single scan [140]. This creative technique is capable of yielding rapid spectral output at the cost of a lower sensitivity than the corresponding conventional experiment. On the other hand, the rapid acquisition of multidimensional data renders it ideal for fast kinetic studies on systems that are not concentration-limited [141].

Importantly, the combination of hyperpolarization methods outlined in Sections 3–7 with the fast data collection approaches described here is a powerful tool, and has already yielded intriguing results [142]. This strategy bears unique promise for future synergistic improvements in resolution, sensitivity and data collection speed.

9. Additional techniques of potential future relevance

The NMR analysis of liquids is sometimes preceded by a spin hyperpolarization step in the solid or gas phase, as in the dissolution DNP and optical pumping approaches. Thus it is conceivable to anticipate that additional methods, presently employed to hyperpolarize non-liquid samples, may in the future gain additional ground and become amenable to the analysis of more wide-ranging classes of molecules by liquid-state NMR. These methodologies include solid-state photo-CIDNP [99], solid-state DNP [36], the Haupt effect [143], transfer of rotational to nuclear spin polarization [144] and microwave-induced optical nuclear polarization (MIONP) [145].

In addition, nontraditional detection schemes have already succeeded or bear future promise to enhance NMR sensitivity in liquids. In optical magnetometry, for instance, the precession of laser-polarized alkali atoms is probed by laser light to detect small local magnetic fields below femtoTesla arising from the NMR samples [146,147]. Alternatively, superconducting quantum interference devices (SQUID) are able to detect magnetic flux, rather than the rates of magnetic flux change [148]. Both optical magnetometry and SQUID detection are actively used in zero-field and low-field NMR of liquids [112,149].

In addition, nuclear spin-induced optical rotation (NSOR) has been used to measure variations in the degree of light polarization to detect nuclear spins of liquid water or liquid ^{129}Xe [150]. Lastly, remote-detection schemes where the spectral information is encoded in one coil and detected in a different coil with optimized filling factor can potentially provide large signal enhancements for ^{129}Xe in liquids [151].

Remarkably, magnetic resonance force microscopy [152] can detect less than 100 nuclear spins of biologically relevant solids by sensing the forces generated by the nuclear magnetic moments of the sample. Finally, the influence of microwave irradiation (which saturates the $T_x \leftrightarrow T_z$ and $T_y \leftrightarrow T_z$ triplet-sublevel transitions) on single-molecule fluorescence enables the indirect detection of the nuclear magnetic moments of the sample at the single-molecule level [153,154]. The nuclear magnetic moments are coupled to the photoexcited electronic states via the hyperfine interaction, which enables the indirect detection of magnetic resonance by fluorescence.

10. Conclusions

In summary, as shown in the side-by-side comparisons provided in Table 1, the leading techniques capable of improving NMR sensitivity in solution have been able to reach amazing results over the last few years, and have several clear advantages. On the other hand, a lot of work still needs to be done, given the few disadvantages. The shortcomings of the methods pose some limits to their applicability to a wide number of NMR-active nuclei and complex biomolecules as well as, in some cases, to long-term data collection. Despite these undeniable challenges, however, progress is happening fast and we anticipate many further exciting advances in future years.

Acknowledgments

We are grateful to Thad Walker, Charlie Fry, Milo Westler, Marco Tonelli and Zachary Deland for useful discussions. This research was supported by NIH Grant R21AI08851 and a UW-Madison Graduate School grant to S.C. In addition, Y.O. is the recipient of an NIH Molecular Biophysics training fellowship.

References

- [1] F. Bloch, W. Hansen, M. Packard, The nuclear induction experiment, *Phys. Rev.* 70 (1946) 474–485.
- [2] L.E. Kay, NMR studies of protein structure and dynamics, *J. Magn. Reson.* 173 (2005) 193–207.
- [3] J. Cavanagh, W.J. Fairbrother, A.G. Palmer III, N.J. Skelton, *Protein NMR Spectroscopy: Principles and Practice*, Academic Press, San Diego, 2007.
- [4] R.R. Ernst, G. Bodenhausen, A. Wokaun, *Principles of Nuclear Magnetic Resonance in One and Two Dimensions*, Oxford University Press, Upper Saddle River, 1989.
- [5] F.J.M. van de Ven, *Multidimensional NMR in Liquids: Basic Principles and Experimental Methods*, Wiley-VCH, New York, 1995.
- [6] R. Freeman, *Handbook of Nuclear Magnetic Resonance*, second ed., Longman, London, 1997.
- [7] A. Abragam, *The Principle of Nuclear Magnetism*, Clarendon Press, Oxford, 1961.

- [8] D.I. Hoult, R. Richards, The signal-to-noise ratio of the nuclear magnetic resonance experiment, *J. Magn. Reson.* 24 (1976) 71–85.
- [9] R.K. Harris, *Nuclear Magnetic Resonance Spectroscopy: A Physicochemical View*, Longman Scientific and Technical, Harlow, 1986.
- [10] T.D.W. Claridge, *High-Resolution NMR Techniques in Organic Chemistry*, second ed., Elsevier, Amsterdam, 2009.
- [11] H. Kovacs, D. Moskau, M. Spraul, Cryogenically cooled probes – a leap in NMR technology, *Prog. Nucl. Magn. Reson. Spectrosc.* 46 (2005) 131–155.
- [12] I. Solomon, Relaxation processes in a system of two spins, *Phys. Rev.* 99 (1955) 559.
- [13] G.A. Morris, R. Freeman, Enhancement of nuclear magnetic resonance signals by polarization transfer, *J. Am. Chem. Soc.* 101 (1979) 760–762.
- [14] A.G. Palmer, J. Cavanagh, P.E. Wright, M. Rance, Sensitivity improvement in proton-detected two-dimensional heteronuclear correlation NMR spectroscopy, *J. Magn. Reson.* 93 (1991) 151–170.
- [15] N.K. Goto, K.H. Gardner, G.A. Mueller, R.C. Willis, L.E. Kay, A robust and cost-effective method for the production of Val, Leu, Ile (δ^1) methyl-protonated ^{15}N -, ^{13}C -, ^2H -labeled proteins, *J. Biomol. NMR* 13 (1999) 369–374.
- [16] M. Kainosho, T. Torizawa, Y. Iwashita, T. Terauchi, A.M. Ono, P. Güntert, Optimal isotope labelling for NMR protein structure determinations, *Nature* 440 (2006) 52–57.
- [17] K.H. Gardner, L.E. Kay, The use of ^2H , ^{13}C , ^{15}N multidimensional NMR to study the structure and dynamics of proteins, *Annu. Rev. Biophys. Biomol. Struct.* 27 (1998) 357–406.
- [18] S. Grzesiek, J. Anglister, H. Ren, A. Bax, ^{13}C line narrowing by ^2H decoupling in $^2\text{H}/^{13}\text{C}/^{15}\text{N}$ enriched proteins. Application to triple resonance 4D J connectivity of sequential amides, *J. Am. Chem. Soc.* 115 (1993) 4369–4370.
- [19] C.J. Jones, C.K. Larive, Could smaller really be better? Current and future trends in high-resolution microcoil NMR spectroscopy, *Anal. Bioanal. Chem.* 402 (2012) 61–68.
- [20] A. Webb, Microcoil nuclear magnetic resonance spectroscopy, *J. Pharm. Biomed. Anal.* 38 (2005) 892–903.
- [21] P. Schanda, B. Brutscher, Very fast two-dimensional NMR spectroscopy for real-time investigation of dynamic events in proteins on the time scale of seconds, *J. Am. Chem. Soc.* 127 (2005) 8014–8015.
- [22] M. Gal, P. Schanda, B. Brutscher, L. Frydman, UltraSOFAST HMQC NMR and the repetitive acquisition of 2D protein spectra at Hz rates, *J. Am. Chem. Soc.* 129 (2007) 1372–1377.
- [23] K. Pervushin, B. Vögeli, A. Eletsky, Longitudinal ^1H relaxation optimization in TROSY NMR spectroscopy, *J. Am. Chem. Soc.* 124 (2002) 12898–12902.
- [24] C. Rossi, Selective relaxation techniques in biological NMR, in: D.M. Grypt, R.K. Harris (Eds.), *Encyclopedia of NMR*, John Wiley & Sons, New York, 1989, pp. 4237–4246.
- [25] A. Bax, R.H. Griffey, B.L. Hawkins, Correlation of proton and nitrogen-15 chemical shifts by multiple quantum NMR, *J. Magn. Reson.* 55 (1983) 301–315.
- [26] K. Pervushin, R. Riek, G. Wider, K. Wüthrich, Attenuated T_2 relaxation by mutual cancellation of dipole–dipole coupling and chemical shift anisotropy indicates an avenue to NMR structures of very large biological macromolecules in solution, *Proc. Natl. Acad. Sci. U. S. A.* 94 (1997) 12366–12371.
- [27] L.E. Kay, Solution NMR spectroscopy of supra-molecular systems, why bother? A methyl-TROSY view, *J. Magn. Reson.* 210 (2011) 159–170.
- [28] M. Salzmann, K. Pervushin, G. Wider, H. Senn, K. Wüthrich, NMR assignment and secondary structure determination of an octameric 110 kDa protein using TROSY in triple resonance experiments, *J. Am. Chem. Soc.* 122 (2000) 7543–7548.
- [29] J.D. Ellett, J.S. Waugh, Chemical shift concertina, *J. Chem. Phys.* 51 (1969) 2851.
- [30] A. Zhuravleva, V.Y. Orekhov, Divided evolution: a scheme for suppression of line broadening induced by conformational exchange, *J. Am. Chem. Soc.* 130 (2008) 3260–3261.
- [31] Y. Li, A.G. Palmer, Narrowing of protein NMR spectral lines broadened by chemical exchange, *J. Am. Chem. Soc.* 132 (2010) 8856–8857.
- [32] S. Meiboom, D. Gill, Modified spin-echo method for measuring nuclear relaxation times, *Rev. Sci. Instrum.* 29 (1958) 688–691.
- [33] J.S. Waugh, L.M. Huber, U. Haeberlen, Approach to high-resolution NMR in solids, *Phys. Rev. Lett.* 20 (1968) 180–182.
- [34] L.L. Lumata, M.E. Merritt, C.R. Malloy, A.D. Sherry, J. van Tol, L. Song, Z. Kovacs, Dissolution DNP-NMR spectroscopy using galvinoxyl as a polarizing agent, *J. Magn. Reson.* 227 (2012) 14–19.
- [35] A.W. Overhauser, Polarization of nuclei in metals, *Phys. Rev.* 92 (1953) 411.
- [36] T. Maly, G.T. Debelouchina, V.S. Bajaj, K.N. Hu, C.G. Joo, M.L. Mak-Jurkauskas, J.R. Sirigiri, P.C.A. van der Wel, J. Herzfeld, R.J. Temkin, R.G. Griffin, Dynamic nuclear polarization at high magnetic fields, *J. Chem. Phys.* 128 (2008) 052211.
- [37] J.H. Ardenkjær-Larsen, B. Fridlund, A. Gram, G. Hansson, L. Hansson, M.H. Lerche, R. Servin, M. Thaning, K. Golman, Increase in signal-to-noise ratio of $>10,000$ times in liquid-state NMR, *Proc. Natl. Acad. Sci. U. S. A.* 100 (2003) 10158–10163.
- [38] U.L. Gunther, Dynamic nuclear hyperpolarization in liquids, *Top. Curr. Chem.* 335 (2013) 23–69.
- [39] P. Miéville, S. Jannin, G. Bodenhausen, Relaxometry of insensitive nuclei: optimizing dissolution dynamic nuclear polarization, *J. Magn. Reson.* 210 (2011) 137–140.
- [40] P. Miéville, P. Ahuja, R. Sarkar, S. Jannin, P.R. Vasos, S. Gerber-Lemaire, M. Mishkovsky, A. Comment, R. Gruetter, O. Ouari, P. Tordo, G. Bodenhausen, Scavenging free radicals to preserve enhancement and extend relaxation times in NMR using dynamic nuclear polarization, *Angew. Chem., Int. Ed.* 122 (2010) 6318–6321.
- [41] J. Leggett, R. Hunter, J. Granwehr, R. Panek, A.J. Perez-Linde, A.J. Horsewill, J. McMaster, G. Smith, W. Kockenberger, A dedicated spectrometer for dissolution DNP NMR spectroscopy, *Phys. Chem. Chem. Phys.* 12 (2010) 5883–5892.
- [42] M. Carravetta, O.G. Johannessen, M.H. Levitt, Beyond the T-1 limit: singlet nuclear spin states in low magnetic fields, *Phys. Rev. Lett.* 92 (2004).
- [43] M. Carravetta, M.H. Levitt, Long-lived nuclear spin states in high-field solution NMR, *J. Am. Chem. Soc.* 126 (2004) 6228–6229.
- [44] M.H. Levitt, Singlet nuclear magnetic resonance, *Annu. Rev. Phys. Chem.* 63 (2012) 89–105.
- [45] W.S. Warren, E. Jenista, R.T. Branca, X. Chen, Increasing hyperpolarized spin lifetimes through true singlet eigenstates, *Science* 323 (2009) 1711–1714.
- [46] M. Carravetta, M.H. Levitt, Theory of long-lived nuclear spin states in solution nuclear magnetic resonance. I. Singlet states in low magnetic field, *J. Chem. Phys.* 122 (2005) 214505.
- [47] P.R. Vasos, A. Comment, R. Sarkar, P. Ahuja, S. Jannin, J.P. Ansermet, J.A. Konter, P. Haulte, B. van den Brandt, G. Bodenhausen, Long-lived states to sustain hyperpolarized magnetization, *Proc. Natl. Acad. Sci. U. S. A.* 106 (2009) 18469–18473.
- [48] L. Lumata, S.J. Ratnakar, A. Jindal, M. Merritt, A. Comment, C. Malloy, A.D. Sherry, Z. Kovacs, BDPA: an efficient polarizing agent for fast dissolution dynamic nuclear polarization NMR spectroscopy, *Chem. Eur. J.* 17 (2011) 10825–10827.
- [49] S. Jannin, A. Bornet, S. Colombo, G. Bodenhausen, Low-temperature cross polarization in view of enhancing dissolution dynamic nuclear polarization in NMR, *Chem. Phys. Lett.* 517 (2011) 234–236.
- [50] M. Batel, M. Krajewski, A. Däpp, A. Hunkeler, B.H. Meier, S. Kozierke, M. Ernst, Dissolution dynamic nuclear polarization efficiency enhanced by Hartmann–Hahn cross polarization, *Chem. Phys. Lett.* 554 (2012) 72–76.
- [51] A. Bornet, R. Melzi, A.J. Perez Linde, P. Haulte, B. van den Brandt, S. Jannin, G. Bodenhausen, Boosting dissolution dynamic nuclear polarization by cross polarization, *J. Phys. Chem. Lett.* 4 (2012) 111–114.
- [52] J.W. Gordon, S.B. Fain, I.J. Rowland, Effect of lanthanide ions on dynamic nuclear polarization enhancement and liquid-state T_1 relaxation, *Magn. Reson. Med.* 68 (2012) 1949–1954.
- [53] H. Zeng, S. Bowen, C. Hilty, Sequentially acquired two-dimensional NMR spectra from hyperpolarized sample, *J. Magn. Reson.* 199 (2009) 159–165.
- [54] M. Mishkovsky, L. Frydman, Progress in hyperpolarized ultrafast 2D NMR spectroscopy, *ChemPhysChem* 9 (2008) 2340–2348.
- [55] G. Zhang, F. Schilling, S.J. Glaser, C. Hilty, Chemical shift correlations from hyperpolarized NMR using a single SHOT, *Anal. Chem.* 85 (2013) 2875–2881.
- [56] K.J. Donovan, L. Frydman, HyperSPASM NMR: a new approach to single-shot 2D correlations on DNP-enhanced samples, *J. Magn. Reson.* 225 (2012) 115–119.
- [57] H.-Y. Chen, C. Hilty, Hyperpolarized Hadamard spectroscopy using flow NMR, *Anal. Chem.* 85 (2013) 7385–7390.
- [58] C.-G. Joo, K.-N. Hu, J.A. Bryant, R.G. Griffin, In situ temperature jump high-frequency dynamic nuclear polarization experiments: enhanced sensitivity in liquid-state NMR spectroscopy, *J. Am. Chem. Soc.* 128 (2006) 9428–9432.
- [59] K. Golman, M. Lerche, R. Pehrson, J.H. Ardenkjær-Larsen, Metabolic imaging by hyperpolarized ^{13}C magnetic resonance imaging for in vivo tumor diagnosis, *Cancer Res.* 66 (2006) 10855–10860.
- [60] S. Bowen, C. Hilty, Time-resolved dynamic nuclear polarization enhanced NMR spectroscopy, *Angew. Chem., Int. Ed.* 120 (2008) 5313–5315.
- [61] P.R. Jensen, S. Meier, J.H. Ardenkjær-Larsen, J.Ø. Duus, M. Karlsson, M.H. Lerche, Detection of low-populated reaction intermediates with hyperpolarized NMR, *Chem. Commun.* (2009) 5168–5170.
- [62] M.H. Lerche, S. Meier, P.R. Jensen, H. Baumann, B.O. Petersen, M. Karlsson, J.Ø. Duus, J.H. Ardenkjær-Larsen, Study of molecular interactions with ^{13}C DNP-NMR, *J. Magn. Reson.* 203 (2010) 52–56.
- [63] H.-Y. Chen, M. Ragavan, C. Hilty, Protein folding studied by dissolution dynamic nuclear polarization, *Angew. Chem., Int. Ed.* 52 (2013) 9192–9195.
- [64] K. Haussler, D. Stehlik, Dynamic nuclear polarization in liquids, *Adv. Magn. Reson.* 3 (1968) 79–139.
- [65] L.P. Hwang, J.H. Freed, Dynamic effects of pair correlation functions on spin relaxation by translational diffusion in liquids, *J. Chem. Phys.* 63 (1975) 4017.
- [66] D. Sezer, M.J. Prandolini, T.F. Prisner, Dynamic nuclear polarization coupling factors calculated from molecular dynamics simulations of a nitroxide radical in water, *Phys. Chem. Chem. Phys.* 11 (2009) 6626–6637.
- [67] C. Griesinger, M. Bennati, H. Vieth, C. Luchinat, G. Parigi, P. Höfer, F. Engelke, S. Glaser, V. Denysenkov, T. Prisner, Dynamic nuclear polarization at high magnetic fields in liquids, *Prog. Nucl. Magn. Reson. Spectrosc.* 64 (2012) 4–28.
- [68] V. Denysenkov, M.J. Prandolini, M. Gafurov, D. Sezer, B. Endeward, T.F. Prisner, Liquid state DNP using a 260 GHz high power gyrotron, *Phys. Chem. Chem. Phys.* 12 (2010) 5786–5790.
- [69] S. Korchak, A. Kiryutin, K. Ivanov, A. Yurkovskaya, Y.A. Grishin, H. Zimmermann, H.-M. Vieth, Low-field, time-resolved dynamic nuclear polarization with field cycling and high-resolution NMR detection, *Appl. Magn. Reson.* 37 (2010) 515–537.
- [70] B.D. Armstrong, J. Choi, C. López, D.A. Wesener, W. Hubbell, S. Cavagnero, S. Han, Site-specific hydration dynamics in the nonpolar core of a molten

- globule by dynamic nuclear polarization of water, *J. Am. Chem. Soc.* 133 (2011) 5987–5995.
- [71] P. Neugebauer, J.G. Krummenacker, V.P. Denysenkov, G. Parigi, C. Luchinat, T.F. Prisner, Liquid state DNP of water at 9.2 T: an experimental access to saturation, *Phys. Chem. Chem. Phys.* 15 (2013) 6049–6056.
 - [72] E.R. McCarney, B.D. Armstrong, M.D. Lingwood, S. Han, Hyperpolarized water as an authentic magnetic resonance imaging contrast agent, *Proc. Natl. Acad. Sci. U. S. A.* 104 (2007) 1754–1759.
 - [73] E.R. McCarney, B.D. Armstrong, R. Kausik, S. Han, Dynamic nuclear polarization enhanced nuclear magnetic resonance and electron spin resonance studies of hydration and local water dynamics in micelle and vesicle assemblies, *Langmuir* 24 (2008) 10062–10072.
 - [74] C.-Y. Cheng, J. Varkey, M.R. Ambrosio, R. Langen, S. Han, Hydration dynamics as an intrinsic ruler for refining protein structure at lipid membrane interfaces, *Proc. Natl. Acad. Sci. U. S. A.* 110 (2013) 16838–16843.
 - [75] J. Bargon, H. Fischer, U. Johnson, Nuclear magnetic resonance emission lines during fast radical reactions. I. Recording methods and examples, *Z. Naturforsch. A* 22 (1967) 1551–1555.
 - [76] H.R. Ward, R.G. Lawler, Nuclear magnetic resonance emission and enhanced absorption in rapid organometallic reactions, *J. Am. Chem. Soc.* 89 (1967) 5518–5519.
 - [77] M. Cocivera, Optically induced overhauser effect in solution. Nuclear magnetic resonance emission, *J. Am. Chem. Soc.* 90 (1968) 3261–3263.
 - [78] R. Kaptein, K. Dijkstra, K. Nicolay, Laser photo-CIDNP as a surface probe for proteins in solution, *Nature* 274 (1978) 293–294.
 - [79] P.J. Hore, R.W. Broadhurst, Photo-CIDNP of biopolymers, *Prog. Nucl. Magn. Reson. Spectrosc.* 25 (1993) 345–402.
 - [80] L.T. Kuhn, Photo-CIDNP NMR spectroscopy of amino acids and proteins, *Top. Curr. Chem.* 338 (2013) 229–300.
 - [81] M. Goez, Photo-CIDNP spectroscopy, in: G.A. Webb (Ed.), *Annual Reports on NMR Spectroscopy*, Academic Press, London, 2009, pp. 77–147.
 - [82] R. Kaptein, J.L. Oosterhoff, Chemically induced dynamic nuclear polarization II – (relation with anomalous ESR spectra), *Chem. Phys. Lett.* 4 (1969) 195–197.
 - [83] G.L. Closs, L.E. Closs, Induced dynamic nuclear spin polarization in photoreductions of benzophenone by toluene and ethylbenzene, *J. Am. Chem. Soc.* 91 (1969) 4549–4550.
 - [84] L.T. Muus, P.W. Atkins, K.A. McLauchlan, J.B. Pedersen (Eds.), *Chemically Induced Magnetic Polarization*, Reidel, Dordrecht, 1977.
 - [85] H. Fabian, S. Grosse, M. Onnen, H.-M. Vieth, A. Yurkovskaya, Chemically induced dynamic nuclear polarization (CIDNP) in the photoreaction of N-acetyl histidine, tyrosine, and tryptophan with 2,2'-dipyridyl and its dependence on the magnetic field, *RIKEN Rev.* 44 (2002) 134–136.
 - [86] S. Grosse, A.V. Yurkovskaya, J. Lopez, H.-M. Vieth, Field dependence of chemically induced dynamic nuclear polarization (CIDNP) in the photoreaction of N-acetyl histidine with 2,2'-dipyridyl in aqueous solution, *J. Chem. Phys. A* 105 (2001) 6311–6319.
 - [87] K.L. Ivanov, H.-M. Vieth, K. Miesel, A.V. Yurkovskaya, R.Z. Sagdeev, Investigation of the magnetic field dependence of CIDNP in multi-nuclear radical pairs. Part II. Photoreaction of tyrosine and comparison of model calculation with experimental data, *Phys. Chem. Chem. Phys.* 5 (2003) 3470–3480.
 - [88] C.E. Lyon, J.A. Jones, C. Redfield, C.M. Dobson, P.J. Hore, Two-dimensional 15N-1H photo-CIDNP as a surface probe of native and partially structured proteins, *J. Am. Chem. Soc.* 121 (1999) 6505–6506.
 - [89] A. Sekhar, S. Cavagnero, 1H photo-CIDNP enhancements in heteronuclear correlation NMR spectroscopy, *J. Phys. Chem. B* 113 (2009) 8310–8318.
 - [90] A. Sekhar, S. Cavagnero, EPIC- and CHANCE-HSQC: two 15N photo-CIDNP-enhanced pulse sequences for the sensitive detection of solvent-exposed tryptophan, *J. Magn. Reson.* 200 (2009) 207–213.
 - [91] J.H. Lee, A. Sekhar, S. Cavagnero, 1H-detected 13C photo-CIDNP as a sensitivity enhancement tool in solution NMR, *J. Am. Chem. Soc.* 133 (2011) 8062–8065.
 - [92] I. Kuprov, P.J. Hore, Chemically amplified 19F-1H nuclear Overhauser effects, *J. Magn. Reson.* 168 (2004) 1–7.
 - [93] K. Maeda, C.E. Lyon, J.J. Lopez, M. Cemazar, C.M. Dobson, P. Hore, Improved photo-CIDNP methods for studying protein structure and folding, *J. Biomol. NMR* 16 (2000) 235–244.
 - [94] P.J. Connolly, J.C. Hoch, Photochemical degradation of tryptophan residues during CIDNP experiments, *J. Magn. Reson.* 95 (1991) 165–173.
 - [95] J.H. Lee, S. Cavagnero, A novel tri-enzyme system in combination with laser-driven NMR enables efficient nuclear polarization of biomolecules in solution, *J. Phys. Chem. B* 117 (2013) 6069–6081.
 - [96] A.S. Kiryutin, S.E. Korchak, K.L. Ivanov, A.V. Yurkovskaya, H.-M. Vieth, Creating long-lived spin states at variable magnetic field by means of photochemically induced dynamic nuclear polarization, *J. Phys. Chem. Lett.* 3 (2012) 1814–1819.
 - [97] M. Goez, I. Kuprov, K. Hun Mok, P. Hore, Novel pulse sequences for time-resolved photo-CIDNP, *Mol. Phys.* 104 (2006) 1675–1686.
 - [98] E. Daviso, G.J. Janssen, A. Alia, G. Jeschke, J. Matysik, M. Tessari, A 10,000-fold nuclear hyperpolarization of a membrane protein in the liquid phase via solid-state mechanism, *J. Am. Chem. Soc.* 133 (2011) 16754–16757.
 - [99] S.S. Thamarath, J. Heberle, P.J. Hore, T. Kottke, J.R. Matysik, Solid-state photo-CIDNP effect observed in phototropin LOV1-C57S by 13C magic-angle spinning NMR spectroscopy, *J. Am. Chem. Soc.* 132 (2010) 15542–15543.
 - [100] G. Jeschke, J. Matysik, A reassessment of the origin of photochemically induced dynamic nuclear polarization effects in solids, *Chem. Phys.* 294 (2003) 239–255.
 - [101] J. Natterer, J. Bargon, Parahydrogen induced polarization, *Prog. Nucl. Magn. Reson. Spectrosc.* 31 (1997) 293–315.
 - [102] S.B. Duckett, C.J. Sleigh, Applications of the parahydrogen phenomenon: a chemical perspective, *Prog. Nucl. Magn. Reson. Spectrosc.* 34 (1999) 71–92.
 - [103] C.R. Bowers, D. Weitekamp, Parahydrogen and synthesis allow dramatically enhanced nuclear alignment, *J. Am. Chem. Soc.* 109 (1987) 5541–5542.
 - [104] M.G. Pravia, D.P. Weitekamp, Net NMR alignment by adiabatic transport of parahydrogen addition products to high magnetic field, *Chem. Phys. Lett.* 145 (1988) 255–258.
 - [105] D. Blazina, S. Duckett, T. Halstead, C. Kozak, R. Taylor, M. Anwar, J. Jones, H. Carteret, Generation and interrogation of a pure nuclear spin state by parahydrogen-enhanced NMR spectroscopy: a defined initial state for quantum computation, *Magn. Reson. Chem.* 43 (2005) 200–208.
 - [106] N.J. Wood, J.A. Brannigan, S.B. Duckett, S.L. Heath, J. Wagstaff, Detection of picomole amounts of biological substrates by para-hydrogen-enhanced NMR methods in conjunction with a suitable receptor complex, *J. Am. Chem. Soc.* 129 (2007) 11012–11013.
 - [107] R.W. Adams, J.A. Aguilar, K.D. Atkinson, M.J. Cowley, P.I. Elliott, S.B. Duckett, G.G. Green, I.G. Khazal, J. López-Serrano, D.C. Williamson, Reversible interactions with para-hydrogen enhance NMR sensitivity by polarization transfer, *Science* 323 (2009) 1708–1711.
 - [108] M.J. Cowley, R.W. Adams, K.D. Atkinson, M.C. Cockett, S.B. Duckett, G.G. Green, J.A. Lohman, R. Kerssebaum, D. Kilgour, R.E. Mewis, Iridium N-heterocyclic carbene complexes as efficient catalysts for magnetization transfer from para-hydrogen, *J. Am. Chem. Soc.* 133 (2011) 6134–6137.
 - [109] S. Glöggler, R. Müller, J. Colell, M. Emondts, M. Dabrowski, B. Blümich, S. Appelt, Para-hydrogen induced polarization of amino acids, peptides and deuterium-hydrogen gas, *Phys. Chem. Chem. Phys.* 13 (2011) 13759–13764.
 - [110] E.B. Dücker, L.T. Kuhn, K. Münnemann, C. Griesinger, Similarity of SABRE field dependence in chemically different substrates, *J. Magn. Reson.* 214 (2012) 159–165.
 - [111] R.W. Adams, S.B. Duckett, R.A. Green, D.C. Williamson, G.G. Green, A theoretical basis for spontaneous polarization transfer in non-hydrogenative parahydrogen-induced polarization, *J. Chem. Phys.* 131 (2009) 194505.
 - [112] T. Theis, M.P. Ledbetter, G. Kervner, J.W. Blanchard, P.J. Ganssle, M.C. Butler, H.D. Shin, D. Budker, A. Pines, Zero-field NMR enhanced by parahydrogen in reversible exchange, *J. Am. Chem. Soc.* 134 (2012) 3987–3990.
 - [113] T.G. Walker, W. Happer, Spin-exchange optical pumping of noble-gas nuclei, *Rev. Mod. Phys.* 69 (1997) 629.
 - [114] B.M. Goodson, Nuclear magnetic resonance of laser-polarized noble gases in molecules, materials, and organisms, *J. Magn. Reson.* 155 (2002) 157–216.
 - [115] P. Nikolaou, A.M. Coffey, L.L. Walkup, B.M. Gust, N. Whiting, H. Newton, S. Barcus, I. Muradyan, M. Dabaghyan, G.D. Moroz, M.S. Rosen, S. Patz, M.J. Barlow, E.Y. Chekmenev, B.M. Goodson, Near-unity nuclear polarization with an open-source 129Xe hyperpolarizer for NMR and MRI, *Proc. Natl. Acad. Sci. U. S. A.* 110 (2013) 14150–14155.
 - [116] N. Whiting, P. Nikolaou, N.A. Eschmann, B.M. Goodson, M.J. Barlow, Interdependence of in-cell xenon density and temperature during Rb/129Xe spin-exchange optical pumping using VHG-narrowed laser diode arrays, *J. Magn. Reson.* 208 (2011) 298–304.
 - [117] T.G. Walker, Fundamentals of spin-exchange optical pumping, *J. Phys.: Conf. Ser.* 294 (2011) 012001.
 - [118] M.S. Rosen, T.E. Chupp, K.P. Coulter, R.C. Welsh, S.D. Swanson, Polarized 129Xe optical pumping/spin exchange and delivery system for magnetic resonance spectroscopy and imaging studies, *Rev. Sci. Instrum.* 70 (1999) 1546–1552.
 - [119] A.-M. Oros, N.J. Shah, Hyperpolarized xenon in NMR and MRI, *Phys. Med. Biol.* 49 (2004) R105.
 - [120] L. Schröder, Xenon for NMR biosensing – inert but alert, *Phys. Med. Biol.* 58 (2013) 3–16.
 - [121] L. Schröder, T. Meldrum, M. Smith, T.J. Lowery, D.E. Wemmer, A. Pines, Temperature response of 129Xe depolarization transfer and its application for ultrasensitive NMR detection, *Phys. Rev. Lett.* 100 (2008) 257603.
 - [122] Y.-Q. Song, Spin polarization-induced nuclear Overhauser effect: an application of spin-polarized xenon and helium, *Concepts Magn. Reson.* 12 (2000) 6–20.
 - [123] A. Cherubini, A. Bifone, Hyperpolarized xenon in biology, *Prog. Nucl. Magn. Reson. Spectrosc.* 42 (2003) 1–30.
 - [124] E. Brunner, Enhancement of surface and biological magnetic resonance using laser-polarized noble gases, *Concepts Magn. Reson.* 11 (1999) 313–335.
 - [125] G. Navon, Y.-Q. Song, T. Rööm, S. Appelt, R.E. Taylor, A. Pines, Enhancement of solution NMR and MRI with laser-polarized xenon, *Science* 271 (1996) 1848–1851.
 - [126] H. Desvaux, L. Dubois, G. Huber, M.L. Quillin, P. Berthault, B.W. Matthews, Dynamics of xenon binding inside the hydrophobic cavity of pseudo-wild-type bacteriophage T4 lysozyme explored through xenon-based NMR spectroscopy, *J. Am. Chem. Soc.* 127 (2005) 11676–11683.
 - [127] P. Berthault, G. Huber, P.T. Ha, L. Dubois, H. Desvaux, E. Guittet, Study of the hydrophobic cavity of β -cryptogin through laser-polarized xenon NMR spectroscopy, *ChemBioChem* 7 (2006) 59–64.

- [128] M.M. Spence, S.M. Rubin, I.E. Dimitrov, E.J. Ruiz, D.E. Wemmer, A. Pines, S.Q. Yao, F. Tian, P.G. Schultz, Functionalized xenon as a biosensor, *Proc. Natl. Acad. Sci. U. S. A.* 98 (2001) 10654–10657.
- [129] P. Berthault, G. Huber, H. Desvaux, Biosensing using laser-polarized xenon NMR/MRI, *Prog. Nucl. Magn. Reson. Spectrosc.* 55 (2009) 35–60.
- [130] L. Schröder, T.J. Lowery, C. Hilty, D.E. Wemmer, A. Pines, Molecular imaging using a targeted magnetic resonance hyperpolarized biosensor, *Science* 314 (2006) 446–449.
- [131] T.K. Stevens, R.M. Ramirez, A. Pines, Nanoemulsion contrast agents with sub-picomolar sensitivity for xenon NMR, *J. Am. Chem. Soc.* (2013).
- [132] K. Kazimierczuk, J. Stanek, A. Zawadzka-Kazimierczuk, W. Koźmiński, Random sampling in multidimensional NMR spectroscopy, *Prog. Nucl. Magn. Reson. Spectrosc.* 57 (2008) 420–434.
- [133] Ě. Kupče, R. Freeman, Projection-reconstruction technique for speeding up multidimensional NMR spectroscopy, *J. Am. Chem. Soc.* 126 (2004) 6429–6440.
- [134] G. Cornilescu, A. Bahrami, M. Tonelli, J.L. Markley, H.R. Eghbalnia, HIFI-C: a robust and fast method for determining NMR couplings from adaptive 3D to 2D projections, *J. Biomol. NMR* 38 (2007) 341–351.
- [135] S.G. Hyberts, K. Takeuchi, G. Wagner, Poisson-gap sampling and forward maximum entropy reconstruction for enhancing the resolution and sensitivity of protein NMR data, *J. Am. Chem. Soc.* 132 (2010) 2145–2147.
- [136] E. Lescop, P. Schanda, R. Rasia, B. Brutscher, Automated spectral compression for fast multidimensional NMR and increased time resolution in real-time NMR spectroscopy, *J. Am. Chem. Soc.* 129 (2007) 2756–2757.
- [137] Ě. Kupče, R. Freeman, Two-dimensional Hadamard spectroscopy, *J. Magn. Reson.* 162 (2003) 300–310.
- [138] B.E. Coggins, R.A. Venters, P. Zhou, Radial sampling for fast NMR: concepts and practices over three decades, *Prog. Nucl. Magn. Reson. Spectrosc.* 57 (2010) 381–419.
- [139] I.C. Felli, B. Brutscher, Recent advances in solution NMR: fast methods and heteronuclear direct detection, *ChemPhysChem* 10 (2009) 1356–1368.
- [140] L. Frydman, T. Scherf, A. Lupulescu, The acquisition of multidimensional NMR spectra within a single scan, *Proc. Natl. Acad. Sci. U. S. A.* 99 (2002) 15858–15862.
- [141] M. Gal, M. Mishkovsky, L. Frydman, Real-time monitoring of chemical transformations by ultrafast 2D NMR spectroscopy, *J. Am. Chem. Soc.* 128 (2006) 951–956.
- [142] L. Frydman, D. Blazina, Ultrafast two-dimensional nuclear magnetic resonance spectroscopy of hyperpolarized solutions, *Nat. Phys.* 3 (2007) 415–419.
- [143] J. Haupt, A new effect of dynamic polarization in a solid obtained by rapid change of temperature, *Phys. Lett. A* 38 (1972) 389–390.
- [144] D. Sofikitis, L. Rubio-Lago, M.R. Martin, D.J.A. Brown, N.C.-M. Bartlett, A.J. Alexander, R.N. Zare, T.P. Rakitzis, Optical control of ground-state atomic orbital alignment: Cl (P) atoms from HCl ($v = 2$, $J = 1$) photodissociation, *J. Chem. Phys.* 127 (2007) 144307.
- [145] H. Van Kesteren, W.T. Wenckebach, J. Schmidt, Production of high, long-lasting, dynamic proton polarization by way of photoexcited triplet states, *Phys. Rev. Lett.* 55 (1985) 1642.
- [146] I. Kominis, T. Kornack, J. Allred, M. Romalis, A subfemtotesla multichannel atomic magnetometer, *Nature* 422 (2003) 596–599.
- [147] D. Budker, M. Romalis, Optical magnetometry, *Nat. Phys.* 3 (2007) 227–234.
- [148] Y.S. Greenberg, Application of superconducting quantum interference devices to nuclear magnetic resonance, *Rev. Mod. Phys.* 70 (1998) 175–222.
- [149] R. McDermott, A.H. Trabesinger, M. Mück, E.L. Hahn, A. Pines, J. Clarke, Liquid-state NMR and scalar couplings in microtesla magnetic fields, *Science* 295 (2002) 2247–2249.
- [150] I. Savukov, S.-K. Lee, M. Romalis, Optical detection of liquid-state NMR, *Nature* 442 (2006) 1021–1024.
- [151] A.J. Moulé, M.M. Spence, S.-I. Han, J.A. Seeley, K.L. Pierce, S. Saxena, A. Pines, Amplification of xenon NMR and MRI by remote detection, *Proc. Natl. Acad. Sci. U. S. A.* 100 (2003) 9122–9127.
- [152] M. Poggio, C. Degen, Force-detected nuclear magnetic resonance: recent advances and future challenges, *Nanotechnology* 21 (2010) 342001.
- [153] J. Köhler, J. Disselhorst, M. Donckers, E. Groenen, J. Schmidt, W. Moerner, Magnetic resonance of a single molecular spin, *Nature* 363 (1993) 242–244.
- [154] J. Wrachtrup, C. Von Borczyskowski, J. Bernard, M. Orritt, R. Brown, Optical detection of magnetic resonance in a single molecule, *Nature* 363 (1993) 244–245.
- [155] T. Pietraß, H.C. Gaede, Optically polarized ^{129}Xe in NMR spectroscopy, *Adv. Mater.* 7 (1995) 826–838.